NASA TECHNICAL NOTE

NASA TN D-5793

NASA TN D-5793

PERFORMANCE AND DEPLOYMENT CHARACTERISTICS OF A TWIN-KEEL PARAWING WITH VARIOUS AMOUNTS AND PERMEABILITIES OF POROUS MATERIAL IN OUTER LOBES

by Harry L. Morgan, Jr.

Langley Research Center
Hampton, Va. 23365

NATIONAL AERONAUTICS AND SPACE ADMINISTRATION • WASHINGTON, D. C. • MAY 1970

1. Report No.	2. Government Accession No.	3. Recipient's Catalog No.
NASA TN D-5793		

4. Title and Subtitle
PERFORMANCE AND DEPLOYMENT CHARACTERISTICS OF A TWIN-KEEL PARAWING WITH VARIOUS AMOUNTS AND PERMEABILITIES OF POROUS MATERIAL IN OUTER LOBES

5. Report Date
May 1970

6. Performing Organization Code

7. Author(s)
Harry L. Morgan, Jr.

8. Performing Organization Report No.
L-6961

9. Performing Organization Name and Address
NASA Langley Research Center
Hampton, Va. 23365

10. Work Unit No.
124-07-20-01-23

11. Contract or Grant No.

12. Sponsoring Agency Name and Address
National Aeronautics and Space Administration
Washington, D.C. 20546

13. Type of Report and Period Covered
Technical Note

14. Sponsoring Agency Code

15. Supplementary Notes

16. Abstract

A low-speed wind-tunnel investigation was conducted to determine the performance and deployment characteristics of a twin-keel all-flexible parawing with various amounts and permeabilities of porous material in the outer lobes. Five models with nominal keel lengths of 6.25 feet (1.91 meters) were constructed and tested. The permeability of the porous materials used in the outer lobes was either 0, 32.0, or 96.0 $ft^3/min/ft^2$ (0, 0.16, or 0.49 $m^3/sec/m^2$) at 1/2 inch (1.27 cm) of water, and the amount of porous material was either 0, 38.9, or 75 percent of the total area of the outer lobes. The test results indicated that the addition of the various amounts and permeabilities of porous materials had little effect on the deployment loads but caused a reduction in flight performance. The increase in permeability caused a reduction in the maximum obtainable lift-drag ratio from 2.90 to 2.13. The increase in the amounts and permeabilities of the porous materials had little effect on the canopy inflation time or on the maximum resultant-force coefficient during deployment.

17. Key Words (Suggested by Author(s))	18. Distribution Statement
Parawing Flexible wing Deployment loads Porous material	Unclassified – Unlimited

19. Security Classif. (of this report)	20. Security Classif. (of this page)	21. No. of Pages	22. Price*
Unclassified	Unclassified	38	$3.00

*For sale by the Clearinghouse for Federal Scientific and Technical Information
Springfield, Virginia 22151

PERFORMANCE AND DEPLOYMENT CHARACTERISTICS OF A TWIN-KEEL PARAWING WITH VARIOUS AMOUNTS AND PERMEABILITIES OF POROUS MATERIAL IN OUTER LOBES

By Harry L. Morgan, Jr.
Langley Research Center

SUMMARY

An investigation was conducted in the 17-foot (5.18-meter) test section of the Langley 300-MPH 7- by 10-foot tunnel to determine the performance and deployment characteristics of a twin-keel all-flexible parawing with various amounts and permeabilities of porous material in the outer lobes. Five models with nominal keel lengths of 6.25 feet (1.91 meters) were constructed and tested. The permeability of the porous materials used in the outer lobes was either 0, 32.0, or 96.0 $ft^3/min/ft^2$ (0, 0.16, or 0.49 $m^3/sec/m^2$) at 1/2 inch (1.27 cm) of water, and the amount of porous material was either 0, 38.9, or 75 percent of the total area of the outer lobes. The test results indicated that the addition of the various amounts and permeabilities of porous materials had little effect on the deployment loads but caused a reduction in flight performance. The increase in permeability caused a reduction in the maximum obtainable lift-drag ratio from 2.90 to 2.13 and a decrease in the range of aft-keel control-line settings required to maintain stable flight in the wind tunnel. For a given permeability, the model with the large porous panels had only a slightly lower maximum lift-drag ratio than the model with the small porous panels; therefore, the increase of the amount of porous material in the area of the outer lobes near the trailing edge had little effect on glide performance. An increase in dynamic pressure (which simulates an increase in wing loading) resulted in a slight reduction in flight performance for all test models except the nonporous model. The increase in the amounts and permeabilities of the porous materials had little effect on the canopy inflation time or on the maximum value of the resultant-force coefficient during deployment.

INTRODUCTION

Many research investigations of all-flexible parawings have been conducted by the National Aeronautics and Space Administration in the past several years. Early work centered around investigations of several different configurations with widely varying geometric, structural, and aerodynamic characteristics. The results of this early work

are presented in references 1 to 3. More recent work has been concerned with studies of the deployment characteristics of all-flexible parawings. This work consisted of both wind-tunnel and free-flight deployment tests of single- and twin-keel parawings. The results of a wind-tunnel investigation of the deployment characteristics of a single-keel parawing are presented in reference 4.

Most all-flexible parawing configurations are characterized by positive and very rapid unreefed deployments which cause deployment loads far in excess of those permissible for recovery of logistic and space payloads. These high loads have led currently to several studies of methods of reefing or venting the canopy to reduce the deployment loads. A review of the development of parachute technology indicated a trend toward an increase in canopy porosity as a means of reducing deployment loads rather than complex and sometimes unreliable reefing schemes. The use of canopy porosity has not been generally applied in the development of parawing technology because of the expected adverse effects on gliding performance. It was felt, however, that an exploratory study should be undertaken to establish the magnitude of the reduction in flight performance and deployment loads associated with an increase in canopy porosity.

The present investigation was conducted to determine the gliding performance and deployment characteristics of a twin-keel all-flexible parawing with various amounts and permeabilities of porous material in the outer lobes. The twin-keel parawing was chosen for this investigation because it has better glide performance characteristics than a single-keel parawing. Also, the addition of porous materials in the outer lobes would constitute less of the total wing area for a twin-keel parawing than for a single-keel parawing and should, therefore, be less detrimental to over-all wing performance. Tuft studies of a twin-keel parawing showed a larger degree of turbulence and flow separation over the outer lobes than over the center lobe; therefore, it was believed that porous materials in the outer lobes rather than in the center lobe would have a less adverse effect on wing performance. Wind-tunnel tests of a series of five twin-keel parawings were made in the 17-foot (5.18-meter) test section of the Langley 300-MPH 7- by 10-foot tunnel.

SYMBOLS

The force and moment coefficients are presented with respect to the wind-axes system. The positive directions of the forces, moment, and angle used in the presentation of the data are shown in figure 1. The model center-of-moment reference point was located at the confluence of the suspension lines held by the line clamping block as illustrated in figure 2. The reference area used in the reduction of the data was the flat-pattern canopy area of 30.17 square feet (2.80 m^2) and the reference chord length was 5.0 feet (1.52 meters). The reference chord length was taken as the theoretical keel

length minus the nose cut-off length. The U.S. Customary System of Units is used and the International System is given in parentheses.

C	fill-time constant, $\frac{t_f V}{l_k}$
C_D	drag coefficient, $\frac{\text{Drag}}{qS}$
C_L	lift coefficient, $\frac{\text{Lift}}{qS}$
C_m	pitching-moment coefficient, $\frac{\text{Pitching moment}}{qSc}$
C_R	resultant-force coefficient, $\sqrt{C_L{}^2 + C_D{}^2}$
c	reference chord length, ft (m)
H_1, H_2, H_3	dimensions of wing-balance attachment apparatus, in. (cm) (see fig. 2)
L/D	lift-drag ratio
l	canopy-suspension-line length, ft (m)
Δl	incremental length of a suspension line, ft (m)
l_k	nominal keel length, ft (m)
Δp	differential pressure across porous materials during permeability tests, inches (cm) of water
q	free-stream dynamic pressure, lb/ft^2 (N/m^2)
S	flat-pattern canopy area, ft^2 (m^2)
t	time, sec
t_f	canopy inflation (fill) time, sec
V	free-stream velocity, $\sqrt{\frac{2q}{\rho}}$, ft/sec (m/sec)
x	distance along keel or leading edge, ft (m) (see fig. 3)

α_w wing angle of attack as measured from vertical to seventh keel line, deg (see fig. 1)

ρ air density, 0.002378 slug/ft^3 (1.226 kg/m^3)

Subscript:

max maximum

DESCRIPTION OF MODELS

Five test models, labeled A, B, C, D, and E, were constructed – a nonporous model and two models each of two additional types. (See fig. 3.) The first type had porous material in the section of the outer lobes from keel line number 5 to 9 and the second type, from keel line number 6 to the trailing edge which composed 38.9 and 75 percent of the total area of the outer lobes, respectively. Each type had one model with low-porosity material in the porous area and one model with high-porosity material. All models had nominal keel lengths of 6.25 feet (1.91 meters) and canopy flat-pattern areas of 30.17 square feet (2.80 m^2). Photographs showing the relative amounts and locations of porous material are presented in figure 4.

The two low-porosity models were constructed of 1.1 oz/yd^2 (0.0372 kg/m^2) porous and nonporous materials, and the two high-porosity models and the nonporous model were constructed of 0.75 oz/yd^2 (0.0254 kg/m^2) porous and nonporous materials. All the materials used were nylon with a ripstop weave, except the high-porosity material which did not have a ripstop weave. The sewn construction details and the construction details of the contoured nose of a twin-keel parawing are presented in figures 5(a) and 5(b), respectively. The nose portion of the center panel of the parawing was contoured to produce an airfoil-like leading edge which, from previous experience, resulted in slightly higher maximum lift-drag ratios than those for a parawing with a plain nose.

The permeabilities of the low- and high-porosity materials were measured on an air permeability machine at differential pressures from 1/2 to 10 inches (1.27 to 25.4 cm) of water and are presented in figure 6 with the corresponding values of effective porosity. The effective porosity values were calculated from the measured values of permeability, based on the assumption of the standard value for the density of air. The term permeability is defined as the measure of the velocity of air through a porous material (which is the same as the volume rate of air flowing through a unit area of porous material) at a given differential pressure across the material, whereas the term effective porosity is defined as the ratio of the velocity of air through a porous material (which is the same as

permeability) to the free-stream velocity $\sqrt{\frac{2\Delta p}{\rho}}$. Detailed discussions of the effects of an increase in effective porosity on the performance of parachutes are presented in reference 5. The materials were not biaxially loaded in tension during the permeability tests; therefore, the values presented in figure 6 are probably lower than those that existed for the materials during the wind-tunnel tests. The permeabilities of the nonporous materials were also measured at 10 inches (25.4 cm) of water, and the 0.75 oz/yd^2 (0.0254 kg/m^2) material had a permeability of 33.5 ft^3/min/ft^2 (0.17 m^3/sec/m^2) and the 1.1 oz/yd^2 (0.0372 kg/m^2) material had zero permeability.

All models were rigged with a 135-pound (600-newton) test dacron line which has low-stretch and low shock-absorbing characteristics compared with that of an equal strength nylon line. Minimizing the line stretch, however, reduced the number of line-length adjustments that had to be made between tests to maintain trim flight.

EXPERIMENTAL TEST PROCEDURES

Performance Tests

The models could not be conveniently tested in the wind tunnel with a single confluence-point suspension system as used in many free-flight tests because the models had neutral roll stability and were unable to maintain an upright position in the wind tunnel. (This condition is not to be confused with the free-flight case in which the freedom of the wing to sideslip plus the stabilizing effect of the payload provide much of the positive roll stability.) To obtain tunnel data, the single confluence-point suspension system was modified by moving the attachment points of the wing-tip control lines outboard to stabilize the model in roll attitude. The attachment points of the wing-tip and aft-keel control lines were also moved rearward to increase the model stability in pitch attitude further. The detailed dimensions of the wing-balance attachment apparatus (T-bar) are given in figure 2 and photographs of the tunnel setup for the performance tests are presented in figure 7(a).

Before testing, the suspension-line lengths for each wing were adjusted until the model had attained the lowest wing angle of attack without collapsing the nose and, at the same time, maintained a smooth canopy shape. The suspension-line lengths for the performance tests, including the initial control-line settings, are listed in table I. During the tests the aft-keel and/or the wing-tip control-line lengths were adjusted to change the model attitude relative to the wind direction. Data were taken through a wing angle-of-attack range which was usually limited at the low end (highest lift-drag ratio) by the angle for partial nose collapse and at the high end by the angle at which excessive longitudinal and lateral oscillations occurred. Tests were also made at several tunnel dynamic pressures to determine the effects of a variation in wing loading on wing performance.

Deployment Tests

Each of the five test models was deployed in the wind tunnel at various dynamic pressures to determine the force-time history and full canopy inflation time (fill time). The confluence of all the suspension lines was attached to a stationary force-measuring system that held the model and prevented downstream travel after line payout, and provided a constant model velocity relative to the free stream during opening. Since the area of the wing was small compared with the cross-sectional area of the test section, the free-stream velocity remained constant during the wing deployment. This type of deployment technique is referred to as an infinite-mass deployment and is identical to the free-flight deployment of the wing with an infinite-mass payload. According to reference 5, free-flight deployments with wing loadings greater than 30 lb/ft^2 (1436.4 N/m^2) are also considered to be infinite-mass deployments. Since the wing develops the maximum resultant force and the maximum projected wing area at the same instant under infinite-mass conditions, the fill time t_f is defined as the time from start of inflation to the time the wing develops its maximum resultant force. The time in the force time histories presented in this report was nondimensionalized with respect to fill time.

Photographs of the apparatus used to deploy the models in the wind tunnel are presented in figure 7(b). Each model was folded in an accordion fold from nose to trailing edge, inserted into a deployment sleeve, and then packed into a deployment canister. The canister was connected to the model support system by means of a release mechanism that was manually operated from outside the test section. The force required to eject the canister at release was supplied by two elastic cords that were stretched taut with one end of each cord attached to the canister and the other end attached to the downstream sidewalls of the tunnel. Detailed dimensions of the deployment canister and base plate are given in reference 4. Before testing, the control-line lengths were adjusted for trim flight with a single confluence point for all the suspension lines. The control-line lengths used for the deployment tests are listed in table I.

Test Conditions and Corrections

Both the performance and deployment tests were conducted in the 17-foot (5.18-meter) test section of the Langley 300-MPH 7- by 10-foot tunnel. The performance tests were conducted at dynamic pressures of 0.5, 1.0, and 2.0 lb/ft^2 (23.9, 47.9, and 95.8 N/m^2) and the deployment tests, at dynamic pressures of 1.0, 1.5, 2.0, and 2.5 lb/ft^2 (47.9, 71.8, 95.8, and 119.7 N/m^2). Force measurements were taken by a six-component strain-gage balance coupled to an electronic system that read and recorded the voltage outputs from the balance. The electronic system read each component at a sampling rate of 62 samples per second which proved to be adequate for continuous mode recording required during the deployment tests. It was necessary to

resolve the balance normal and side forces into a resultant lift force during the reduction of the deployment data because the wings could not be packed so that the wing would consistently deploy in the same direction.

Jet-boundary corrections to the wing angle of attack and drag coefficients as determined from reference 6 were applied to the performance data but not to the deployment data because it was felt that the corrections would not be valid for dynamic mode data. The blockage corrections were negligible because of the small ratio of the wing area to the cross-sectional area of the test section (approximately 0.11) and were therefore not applied to the data.

RESULTS AND DISCUSSION

Performance Characteristics

The results of the performance tests showed a reduction in the flight performance with an increase in the permeability of the porous materials used in the outer lobes. Summary plots of the maximum obtainable values of the lift-drag ratio and their corresponding lift and drag coefficients are presented in figure 8. The data presented in this figure were taken from the performance data presented in figure 9 which are given as functions of incremental shortening in the aft-keel control lines from their basic lengths (given in table I) for various settings of the wing-tip control lines. The value of $(L/D)_{max}$ decreased from 2.90 to 2.13 as the permeability of the porous materials increased from 0 to 96.0 $ft^3/min/ft^2$ (0 to 0.49 $m^3/sec/m^2$) at 1/2 inch (1.27 cm) of water. The decrease in $(L/D)_{max}$ was a result of both a decrease in lift and an increase in drag. A decrease in both lift and drag was expected because of the increase in effective porosity associated with the increase in permeability; however, there was an increase in drag which was probably the result of an increase in the angle of attack of the wing. Figure 8 shows that, for a given permeability, the model with the large porous panels had only a slightly lower $(L/D)_{max}$ than the model with the small porous panels. This result indicates that the addition of porous material in the area of the wing near the trailing edge of the outer lobes had little effect on the glide performance.

An increase in the permeability of the porous materials also resulted in a decrease in the range of aft-keel control-line settings required to maintain stable flight in the wind tunnel. The test results presented in figure 9 show also that the addition of porous material in the area of the wing near the trailing edge of the outer lobes had little effect on the range of aft-keel control-line lengths required to maintain trim flight in the wind tunnel. Previous free-flight tests of other all-flexible parawing configurations with wind-tunnel riggings often resulted in a range of control-line lengths different from that obtainable in the wind tunnel; however, comparable performance trends observed in wind-tunnel test results of several configurations have also been observed in free-flight test results.

An increase in free-stream dynamic pressure (which simulates an increase in wing loading) caused a general reduction in the lift, drag, and resultant-force coefficients at a constant control-line setting as well as a reduction in the maximum obtainable lift-drag ratio for all the test models except the nonporous model. (See fig. 10.) The decrease in the lift and drag coefficients was expected because of an increase in effective porosity which was caused by an increase in differential pressure with increased dynamic pressure as shown in figure 6. Each model was tested at free-stream dynamic pressures of 0.5, 1.0, and 2.0 lb/ft^2 (23.9, 47.9, and 95.8 N/m^2) and data were taken by varying the aft-keel control-line lengths with the wing-tip control lines set at their basic lengths. The increase in free-stream dynamic pressure had little effect on the range of aft-keel control-line lengths required to maintain stable flight in the tunnel for all the test models.

Deployment Characteristics

The addition of porous material in the outer lobes of the twin-keel parawing had little effect on either the filling time or the maximum resultant-force coefficient developed during deployment. The filling distance for a parawing deployed in the wind tunnel under infinite-mass conditions is equal to the product of the tunnel velocity and the fill time provided the tunnel velocity remains constant during the deployment. Dividing the filling distance by the keel length of the parawing yields a nondimensional parameter that represents the number of keel lengths the wing travels during opening and is defined in this report as the fill-time constant $C = \frac{t_f V}{l_k}$. The variation of fill-time constant with free-stream dynamic pressure for the models tested in this investigation is presented in figure 11. The value of this constant varied from approximately 1.5 to 1.9 with an average value of 1.66 for all the test models. No distinct trend with respect to an increase in permeability could be determined because of the random variation of the constant for each wing.

The nondimensionalized time histories of the lift, drag, and resultant-force coefficients for each test model are presented in figure 12, and the tabulated time histories of the mean curves faired through these data are given in table II. The tabulated data show a slight decrease in the value of the maximum resultant-force coefficient with an increase in permeability. The reduction in $C_{R,max}$ was caused primarily by the reduction in lift coefficient. Since the test results show relatively small differences in the values of the fill-time constants and maximum resultant-force coefficients, it can be concluded that the addition of porous materials in the outer lobes would have little effect on the free-flight deployment loads of larger size twin-keel wings with similar distributions of porous material.

CONCLUSIONS

The results of a wind-tunnel investigation of a twin-keel all-flexible parawing with various amounts and permeabilities of porous materials in the outer lobes may be summarized as follows:

1. The addition of the various amounts and permeabilities of porous material in the outer lobes caused a reduction in the performance characteristics of the twin-keel parawing. The maximum obtainable lift-drag ratio decreased from 2.90 to 2.13 as the permeability of the porous materials increased from 0 to 96.0 $ft^3/min/ft^2$ (0 to 0.49 $m^3/sec/m^2$) at 1/2 inch (1.27 cm) of water. The reduction in the maximum lift-drag ratio was caused by a decrease in lift and an increase in drag.

2. For a given permeability, the model with the large porous panels had only a slightly lower maximum lift-drag ratio than the model with small porous panels. This result indicated that the addition of porous materials in the area of the wing near the trailing edge of the outer lobes had little effect on glide performance.

3. An increase in permeability caused a decrease in the range of aft-keel control-line settings required to maintain stable flight in the wind tunnel.

4. An increase in dynamic pressure (which simulates an increase in wing loading) resulted in a reduction in maximum lift-drag ratio and in a decrease in lift, drag, and resultant-force coefficients at a constant control-line setting for all test models except the nonporous model.

5. The addition of porous material in the outer lobes had little effect on the deployment inflation time or on the maximum resultant-force coefficient during deployment. The average filling time was 1.66 times the ratio of keel length to free-stream velocity. The slight reduction in maximum resultant-force coefficient with an increase in material porosity was primarily a result of a reduction in lift coefficient.

Langley Research Center,
National Aeronautics and Space Administration,
Langley Station, Hampton, Va., March 16, 1970.

REFERENCES

1. Libbey, Charles E.; Ware, George M.; and Naeseth, Rodger L.: Wind-Tunnel Investigation of the Static Aerodynamic Characteristics of an 18-Foot (5.49-Meter) All-Flexible Parawing. NASA TN D-3856, 1967.

2. Naeseth, Rodger L.; and Fournier, Paul G.: Low-Speed Wind-Tunnel Investigation of Tension-Structure Parawings. NASA TN D-3940, 1967.

3. Ware, George M.: Wind-Tunnel Investigation of the Aerodynamic Characteristics of a Twin-Keel Parawing. NASA TN D-5199, 1969.

4. Gainer, Thomas G.: Investigation of Opening Characteristics of an All-Flexible Parawing. NASA TN D-5031, 1969.

5. Amer. Power Jet Co.: Performance of and Design Criteria for Deployable Aerodynamic Decelerators. ASD-TR-61-579, U.S. Air Force, Dec. 1963. (Available from DDC as AD 429 921.)

6. Gillis, Clarence L.; Polhamus, Edward C.; and Gray, Joseph L., Jr.: Charts for Determining Jet-Boundary Corrections for Complete Models in 7- by 10-Foot Closed Rectangular Wind Tunnels. NACA WR L-123, 1945. (Formerly NACA ARR L5G31.)

TABLE I.- LINE ATTACHMENT LOCATIONS AND LINE LENGTHS

Keel		Leading edge		Keel		Leading edge	
x/l_k	l/l_k	x/l_k	l/l_k	x/l_k	l/l_k	x/l_k	l/l_k
Model A				Model B			
0.267	0.969	0.416	0.953	0.267	0.977	0.416	0.941
.333	.979	.549	.907	.333	.981	.549	.929
.400	.984	.683	.902	.400	.976	.683	.904
.467	.990	.816	.843	.467	.975	.816	.860
.533	.990	.949	.777	.533	.972	.949	.797
.600	.992	[a]1.083	.633	.600	.971	[a]1.083	.677
.667	.988	[b]1.083	.667	.667	.977	[b]1.083	.719
.733	.967			.733	.971		
.800	.963			.800	.963		
.867	.955			.867	.956		
.933	.927			.933	.930		
[a]1.000	.873			[a]1.000	.871		
[b]1.000	.908			[b]1.000	.913		
Model C				Model D			
0.267	0.983	0.416	0.955	0.267	0.982	0.416	0.942
.333	.990	.549	.948	.333	.993	.549	.929
.400	.983	.683	.933	.400	.992	.683	.898
.467	.977	.816	.885	.467	.987	.816	.837
.533	.978	.949	.814	.533	.987	.949	.772
.600	.979	[a]1.083	.672	.600	.986	[a]1.083	.618
.667	.978	[b]1.083	.721	.667	.978	[b]1.083	.655
.733	.972			.733	.971		
.800	.965			.800	.970		
.867	.961			.867	.961		
.933	.944			.933	.949		
[a]1.000	.889			[a]1.000	.881		
[b]1.000	.908			[b]1.000	.931		
Model E							
0.267	0.981	0.416	0.971				
.333	.988	.549	.950				
.400	.985	.683	.922				
.467	.982	.816	.902				
.533	.986	.949	.843				
.600	.985	[a]1.083	.680				
.667	.985	[b]1.083	.735				
.733	.985						
.800	.978						
.867	.965						
.933	.944						
[a]1.000	.917						
[b]1.000	.919						

[a]Performance tests.

[b]Deployment tests.

TABLE II.- TABULATED TIME HISTORIES OF THE MEAN LIFT, DRAG, AND RESULTANT-FORCE COEFFICIENT AND LIFT-DRAG RATIO

t/t_f	C_L	C_D	C_R	L/D	C_L	C_D	C_R	L/D	C_L	C_D	C_R	L/D
	Model A				Model B				Model C			
0	0	0	0	0	0	0	0	0	0	0	0	0
.1	.03	.15	.15	.20	.02	.07	.07	.29	.01	.10	.10	.10
.2	.06	.33	.34	.18	.04	.15	.16	.27	.03	.21	.21	.14
.3	.09	.53	.54	.17	.05	.29	.29	.17	.06	.33	.34	.18
.4	.15	.76	.77	.20	.06	.49	.49	.12	.08	.47	.48	.17
.5	.21	1.07	1.09	.20	.09	.74	.75	.12	.13	.68	.69	.19
.6	.32	1.60	1.63	.20	.11	1.18	1.19	.09	.18	1.02	1.04	.18
.7	.59	2.22	2.30	.27	.21	1.73	1.74	.12	.28	1.44	1.47	.19
.8	.97	2.56	2.74	.38	.43	2.26	2.30	.19	.49	1.93	1.99	.25
.9	1.44	2.78	3.13	.52	.84	2.68	2.81	.31	.81	2.23	2.37	.36
1.0	2.24	2.42	3.30	.93	1.35	2.60	2.93	.52	1.30	2.12	2.49	.61
1.1	2.23	1.67	2.79	1.34	1.71	1.96	2.60	.87	1.52	1.72	2.30	.88
1.2	1.50	.82	1.71	1.83	1.70	1.20	2.08	1.42	1.32	1.16	1.76	1.14
1.3	.99	.36	1.05	2.75	1.22	.65	1.38	1.88	1.00	.63	1.18	1.59
1.4	.64	.20	.67	3.20	.88	.42	.98	2.10	.79	.47	.92	1.68
1.6	.45	.16	.48	2.81	.58	.22	.62	2.64	.60	.32	.68	1.88
1.8	.68	.46	.82	1.49	.54	.23	.59	2.35	.57	.33	.66	1.73
2.0	.87	.78	1.17	1.12	.72	.41	.83	1.76	.68	.47	.83	1.45
2.2	.91	1.04	1.38	.88	.87	.57	1.04	1.53	.80	.51	.95	1.57
2.4	1.19	1.11	1.63	1.07	.95	.55	1.10	1.73	.87	.47	.99	1.85
2.6	1.49	.97	1.78	1.54	.91	.47	1.02	1.94	.83	.42	.93	1.98
2.8	1.39	.68	1.55	2.04	.80	.37	.88	2.16	.75	.40	.85	1.88
3.0	1.03	.40	1.11	2.58	.75	.34	.82	2.21	.72	.34	.80	2.12
3.2	.80	.28	.85	2.86	.75	.30	.81	2.50				
	Model D				Model E							
0	0	0	0	0	0	0	0	0				
.1	.02	.08	.08	.25	.03	.07	.08	.43				
.2	.06	.18	.19	.33	.06	.14	.15	.43				
.3	.08	.29	.30	.28	.08	.22	.23	.36				
.4	.11	.46	.47	.24	.12	.35	.37	.34				
.5	.14	.73	.74	.19	.15	.56	.58	.27				
.6	.21	1.12	1.14	.19	.21	.90	.92	.23				
.7	.38	1.65	1.69	.23	.33	1.33	1.37	.25				
.8	.71	2.16	2.27	.33	.56	1.77	1.86	.32				
.9	1.21	2.51	2.79	.48	.87	2.26	2.42	.38				
1.0	1.82	2.38	3.00	.76	1.29	2.27	2.61	.57				
1.1	2.02	1.86	2.75	1.09	1.60	1.85	2.45	.86				
1.2	1.43	.96	1.72	1.49	1.51	1.24	1.95	1.22				
1.3	.98	.39	1.05	2.51	1.25	.80	1.48	1.56				
1.4	.72	.24	.76	3.00	1.02	.56	1.16	1.82				
1.6	.50	.17	.53	2.94	.65	.34	.73	1.91				
1.8	.57	.25	.62	2.28	.61	.35	.70	1.74				
2.0	.77	.46	.90	1.67	.77	.47	.90	1.64				
2.2	.97	.62	1.15	1.56	.88	.55	1.04	1.60				
2.4	1.11	.69	1.31	1.61	.90	.51	1.03	1.76				
2.6	1.09	.63	1.26	1.73	.87	.44	.97	1.98				
2.8	.95	.48	1.06	1.98	.80	.39	.89	2.05				
3.0	.83	.31	.89	2.68	.78	.38	.87	2.05				
3.2					.79	.39	.88	2.03				
3.4					.80	.38	.89	2.11				

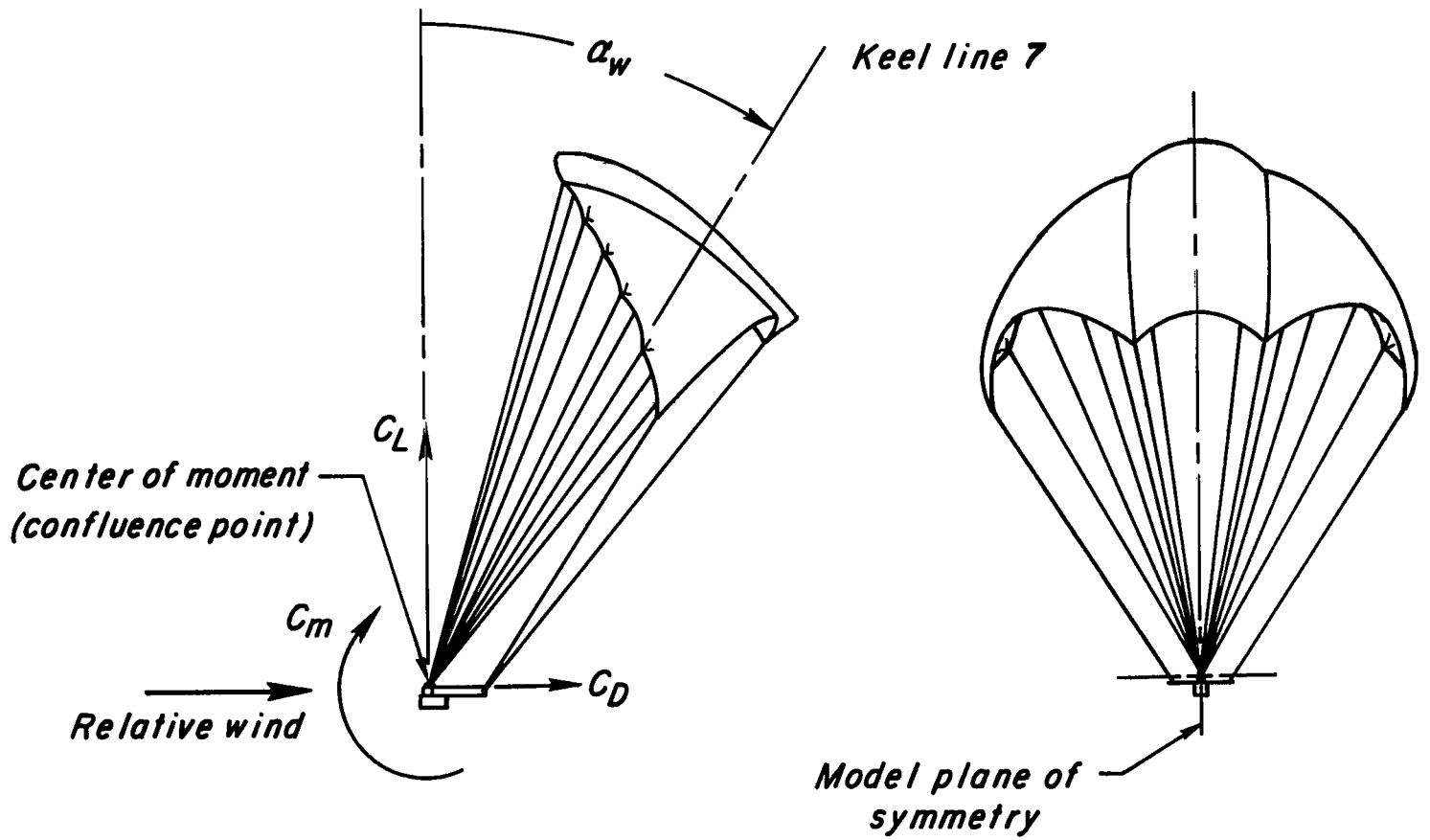

Figure 1.- System of axes and the positive direction of the forces, moment, and angle used in the presentation of the data.

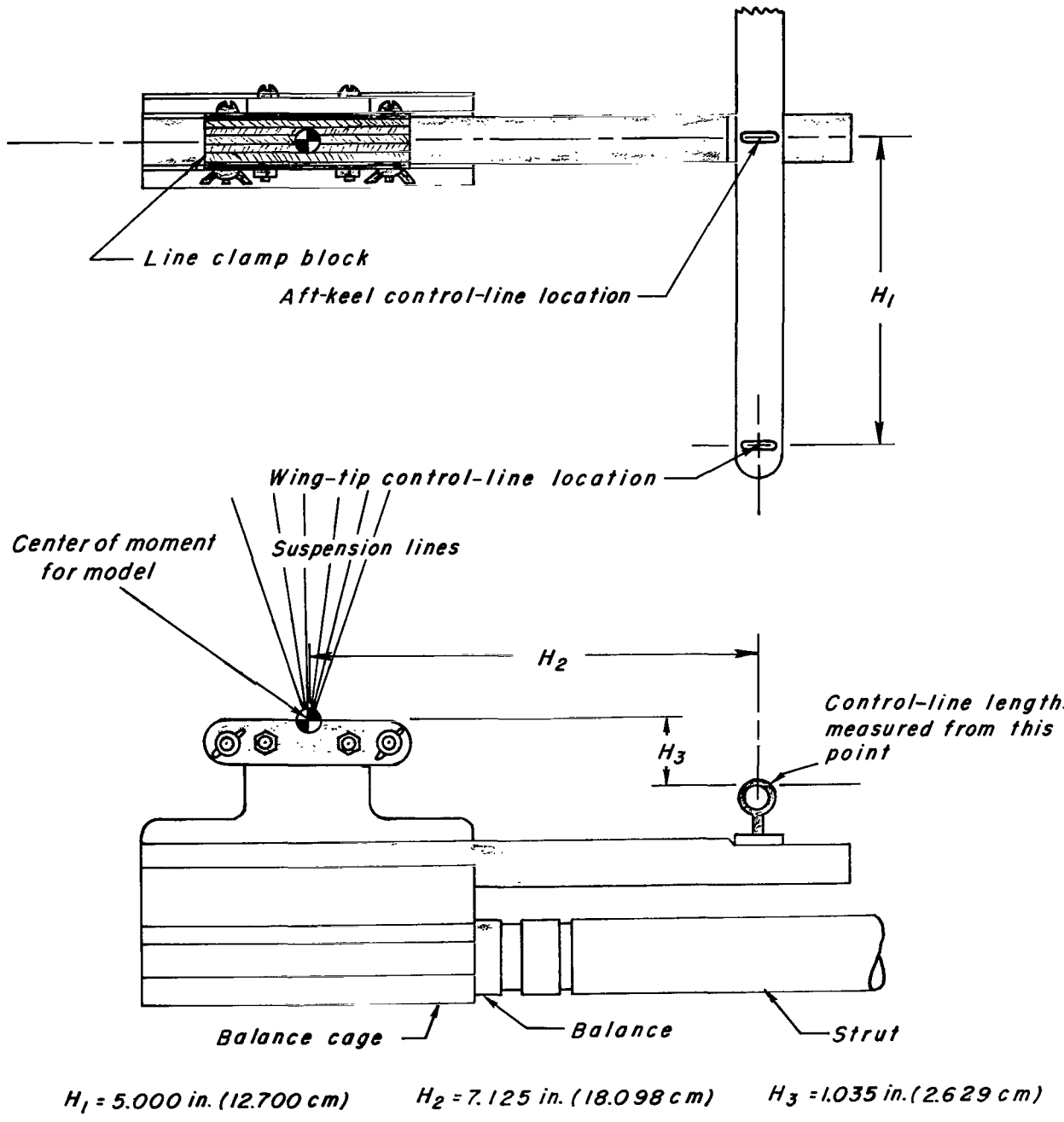

Figure 2.- Details of the wing-balance attachment apparatus (T-bar).

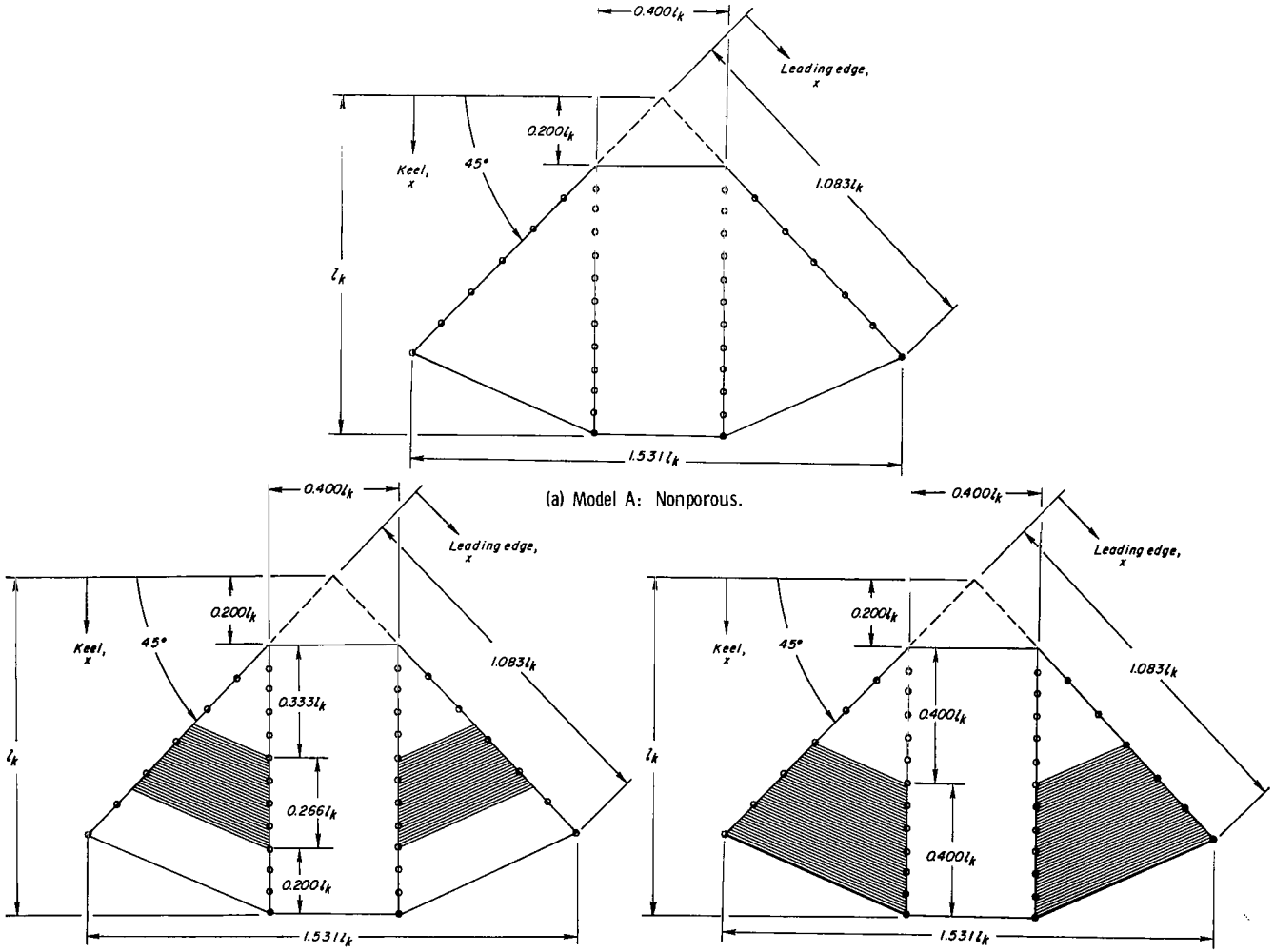

(a) Model A: Nonporous.

(b) Model B: Low-porosity; Model C: High-porosity.

(c) Model D: Low-porosity; Model E: High-porosity.

Figure 3.- Planform details of the test models. Model porosity refers to the porosity of the shaded area.

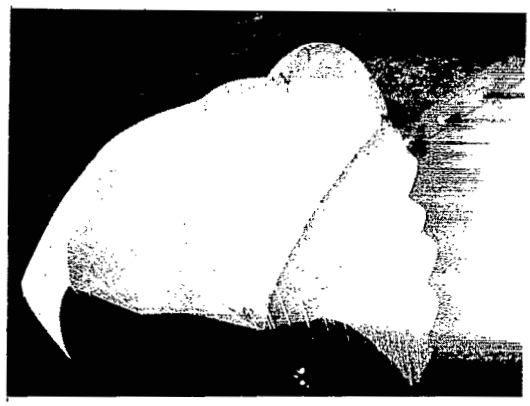

Model A

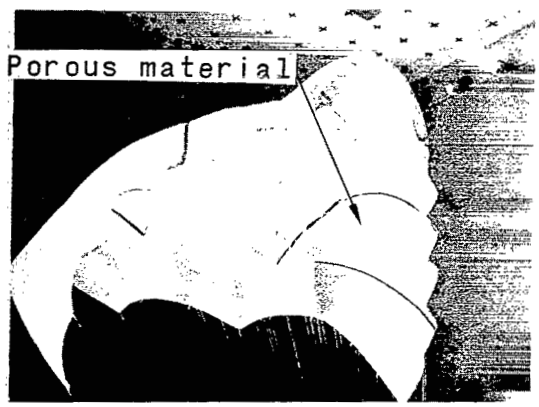

Models B and C

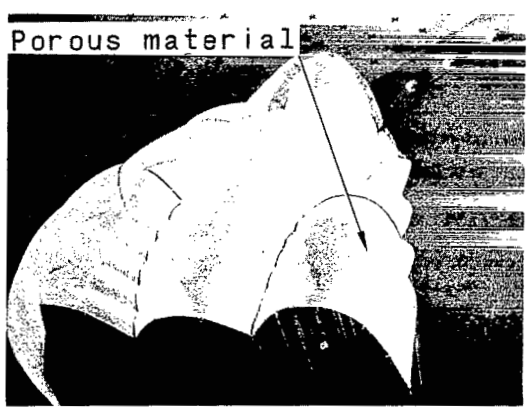

Models D and E

Figure 4.- Photographs of test models taken during performance tests in wind tunnel. L-70-1550

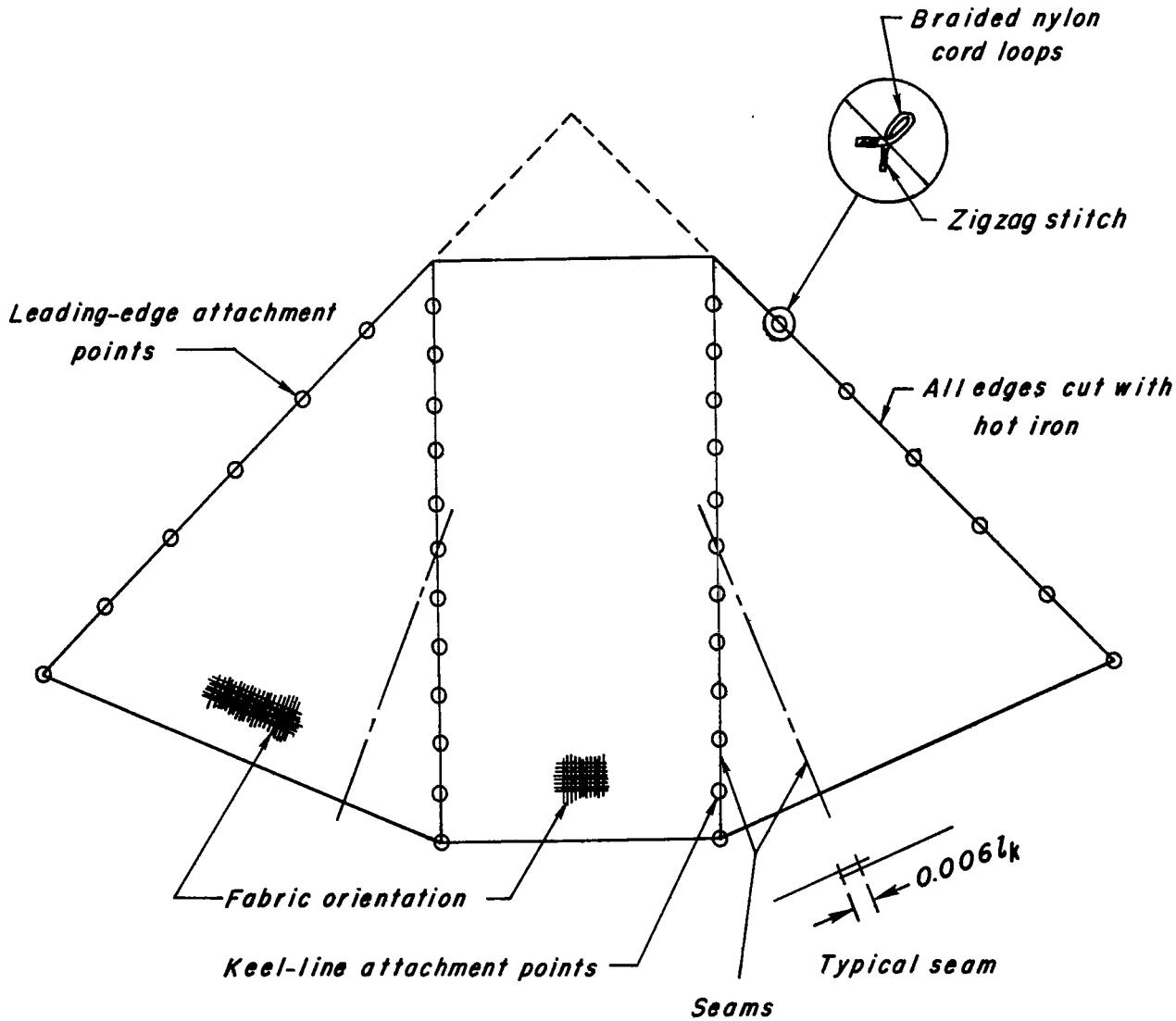

(a) Sewn construction details.

Figure 5.- Construction details of a twin-keel all-flexible parawing.

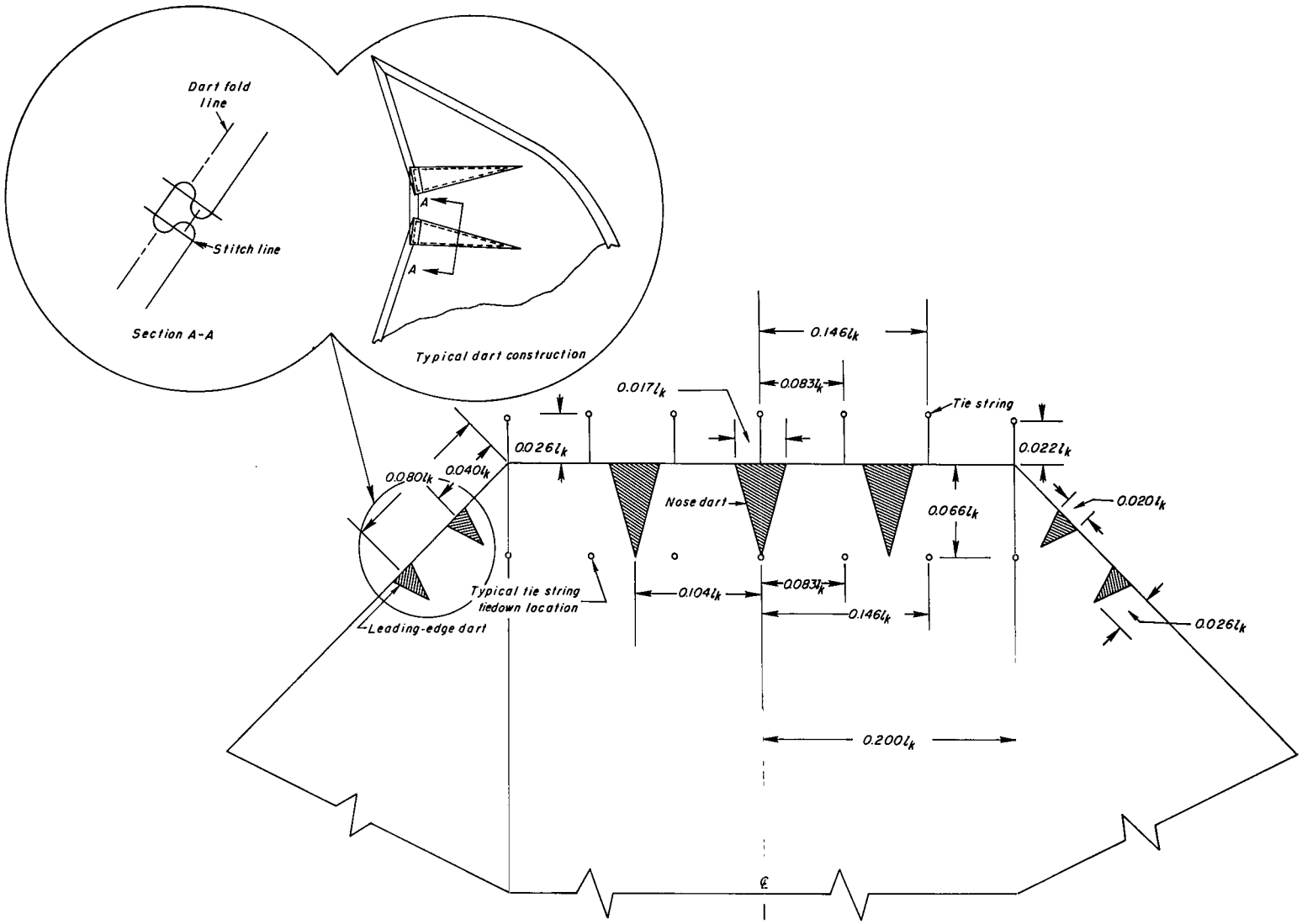

(b) Nose construction details.

Figure 5.- Concluded.

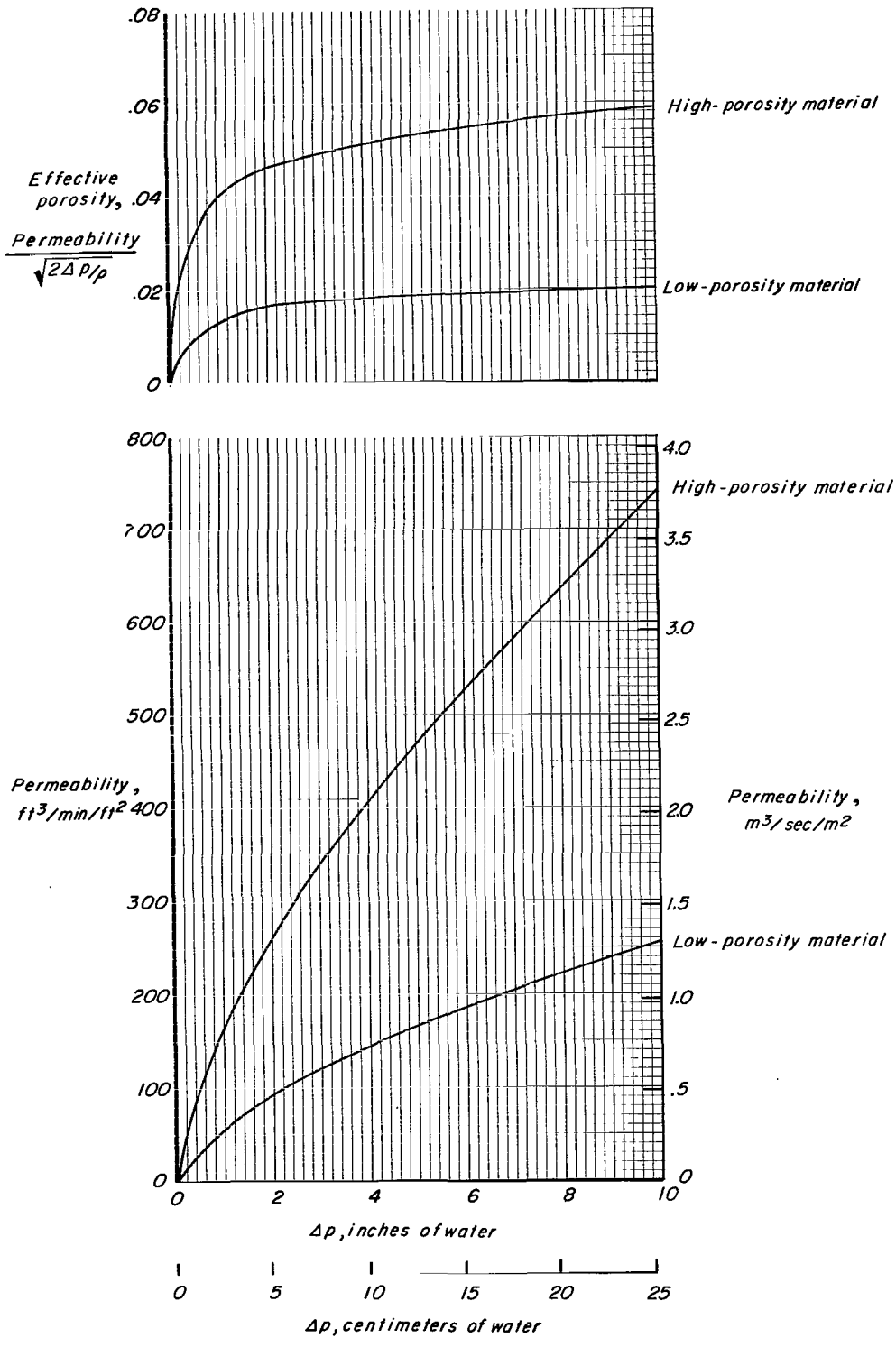

Figure 6.- Permeability and effective porosity of porous materials used in test models.

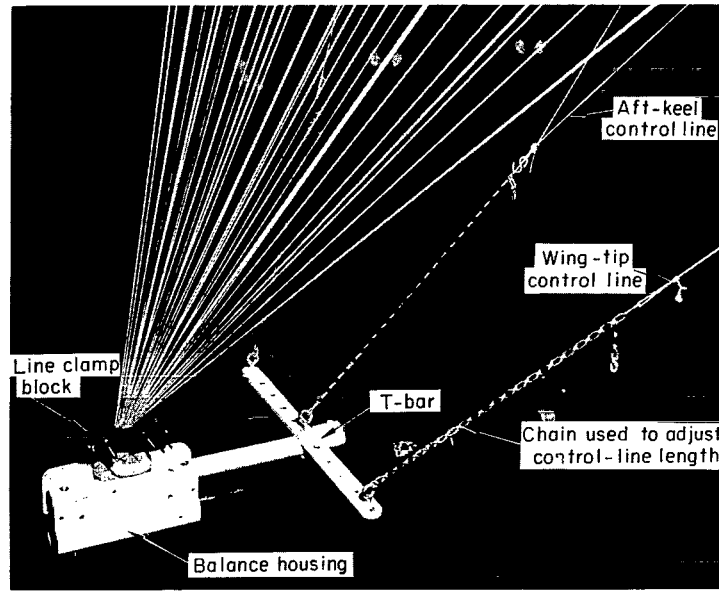

(a) Performance tests.

L-70-1551

Figure 7.- Photographs of the wind-tunnel setups for the performance and deployment tests.

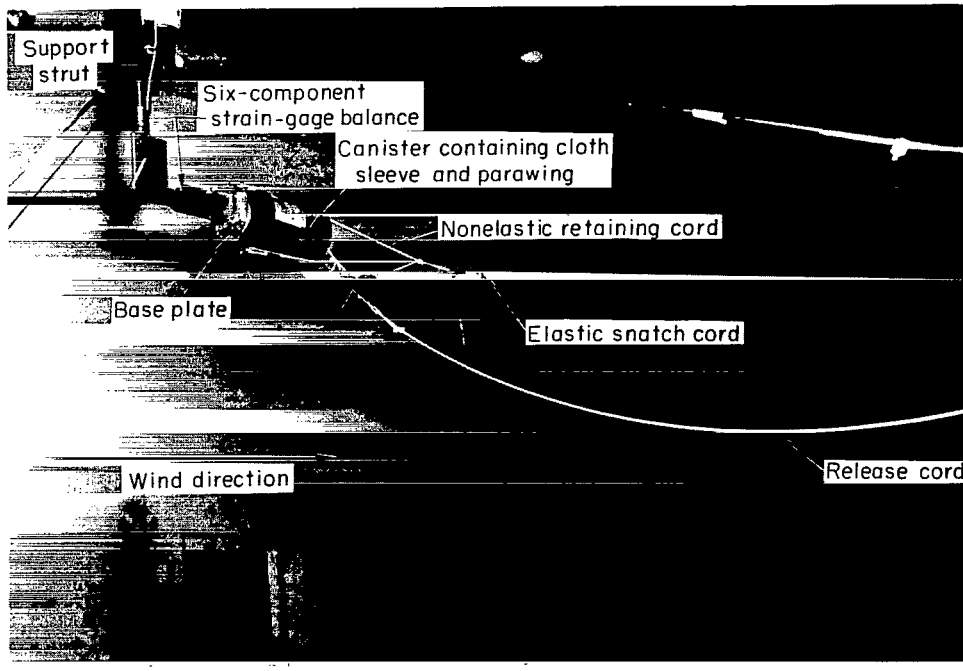

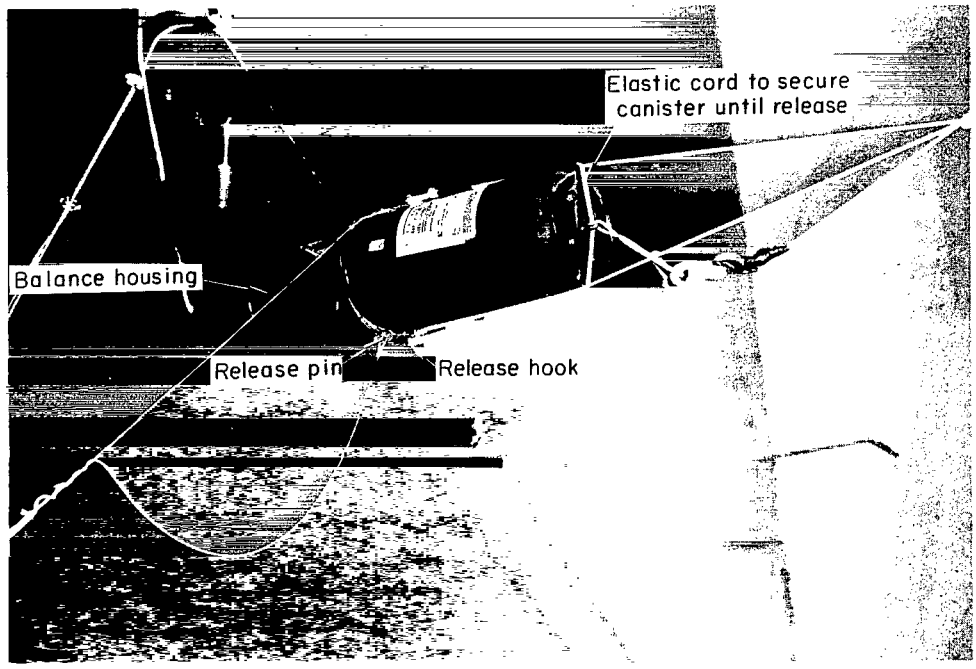

(b) Deployment tests.

Figure 7.- Concluded.

L-70-1552

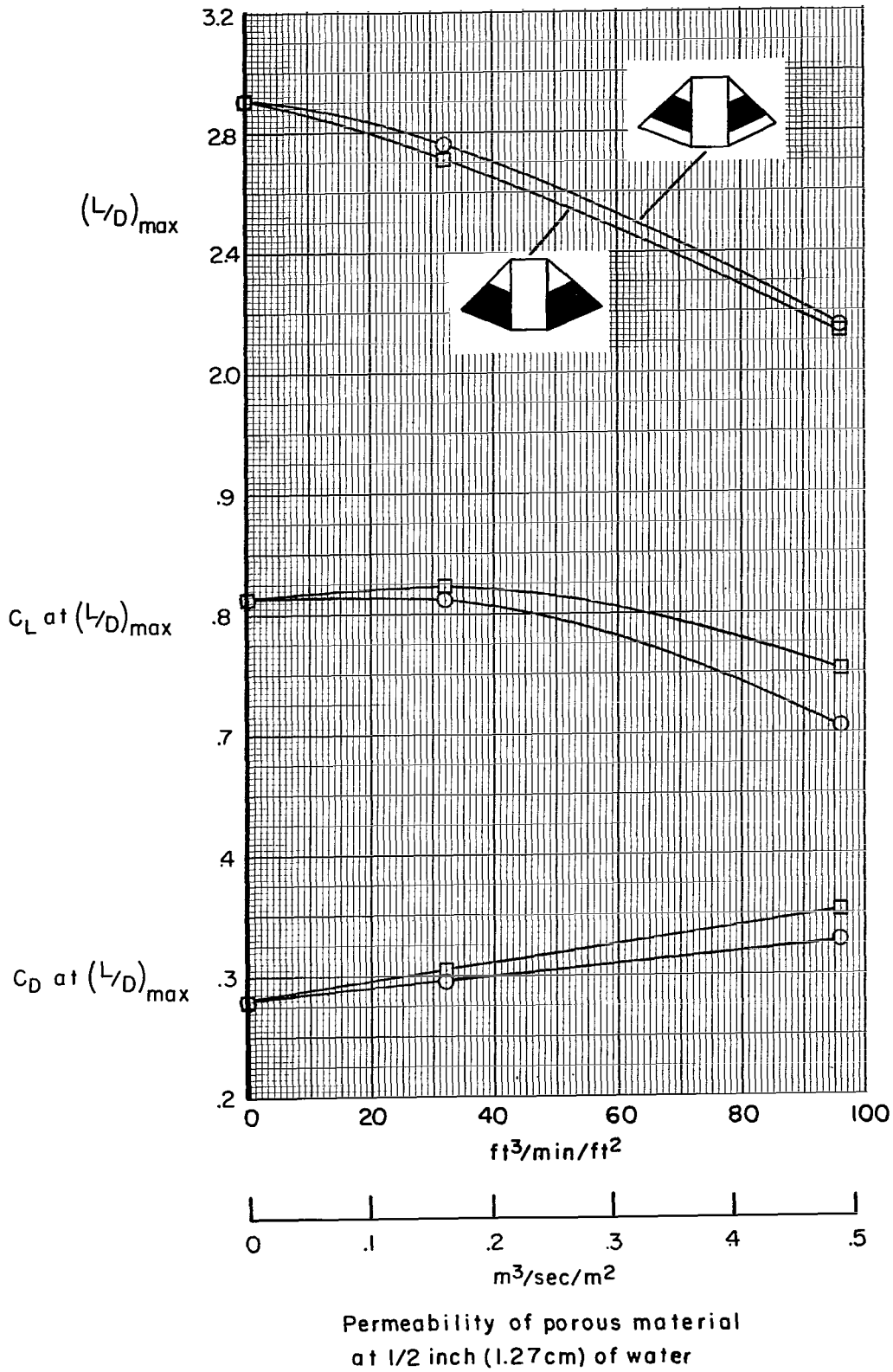

Figure 8.- Variation of $(L/D)_{max}$ with an increase in material porosity.

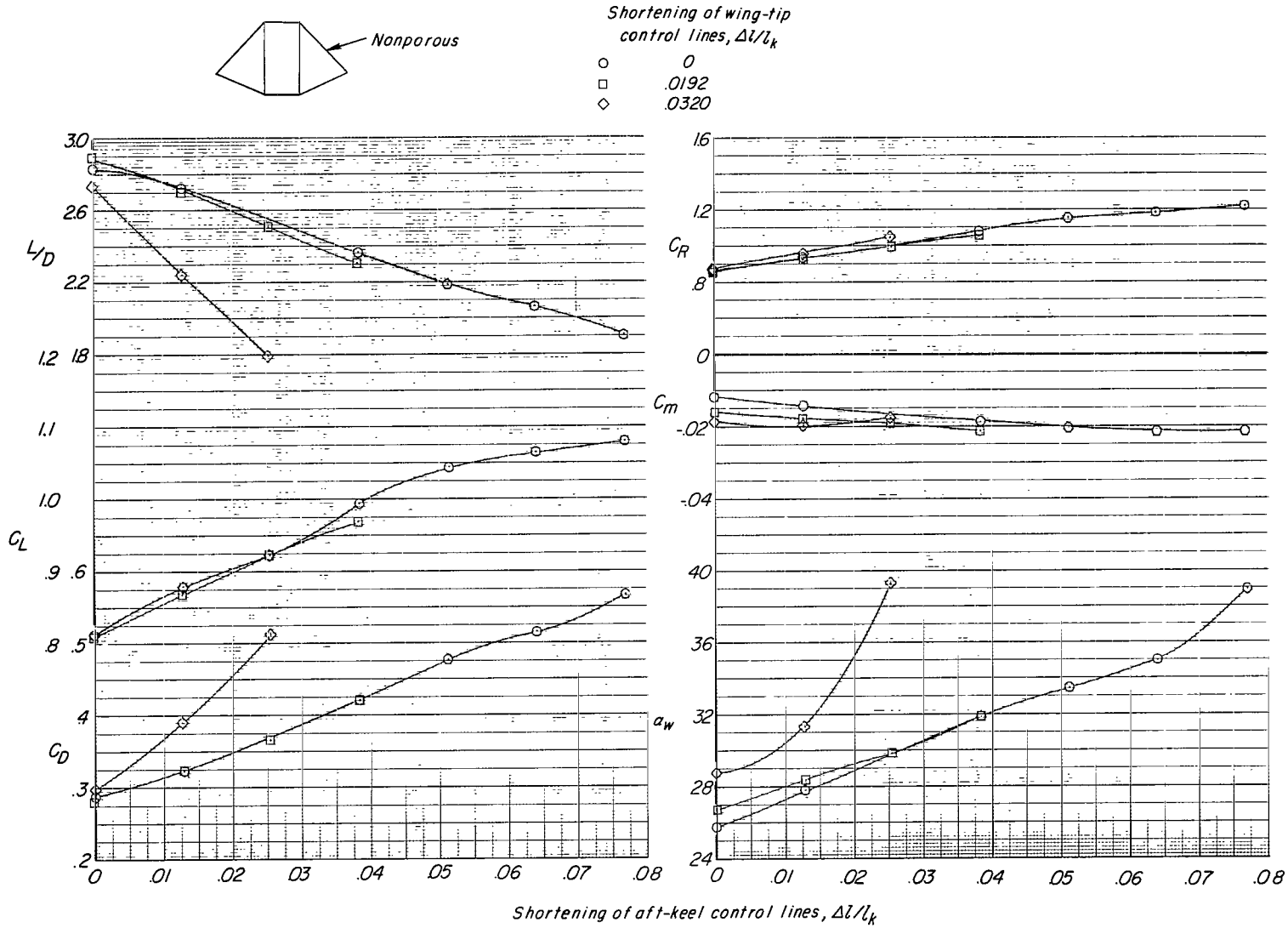

(a) Model A.

Figure 9.- Effects of control-line shortening on the longitudinal aerodynamic characteristics of a twin-keel all-flexible parawing with various amounts and permeabilities of porous material in outer lobes; $q = 1.0$ lb/ft^2 (47.9 N/m^2).

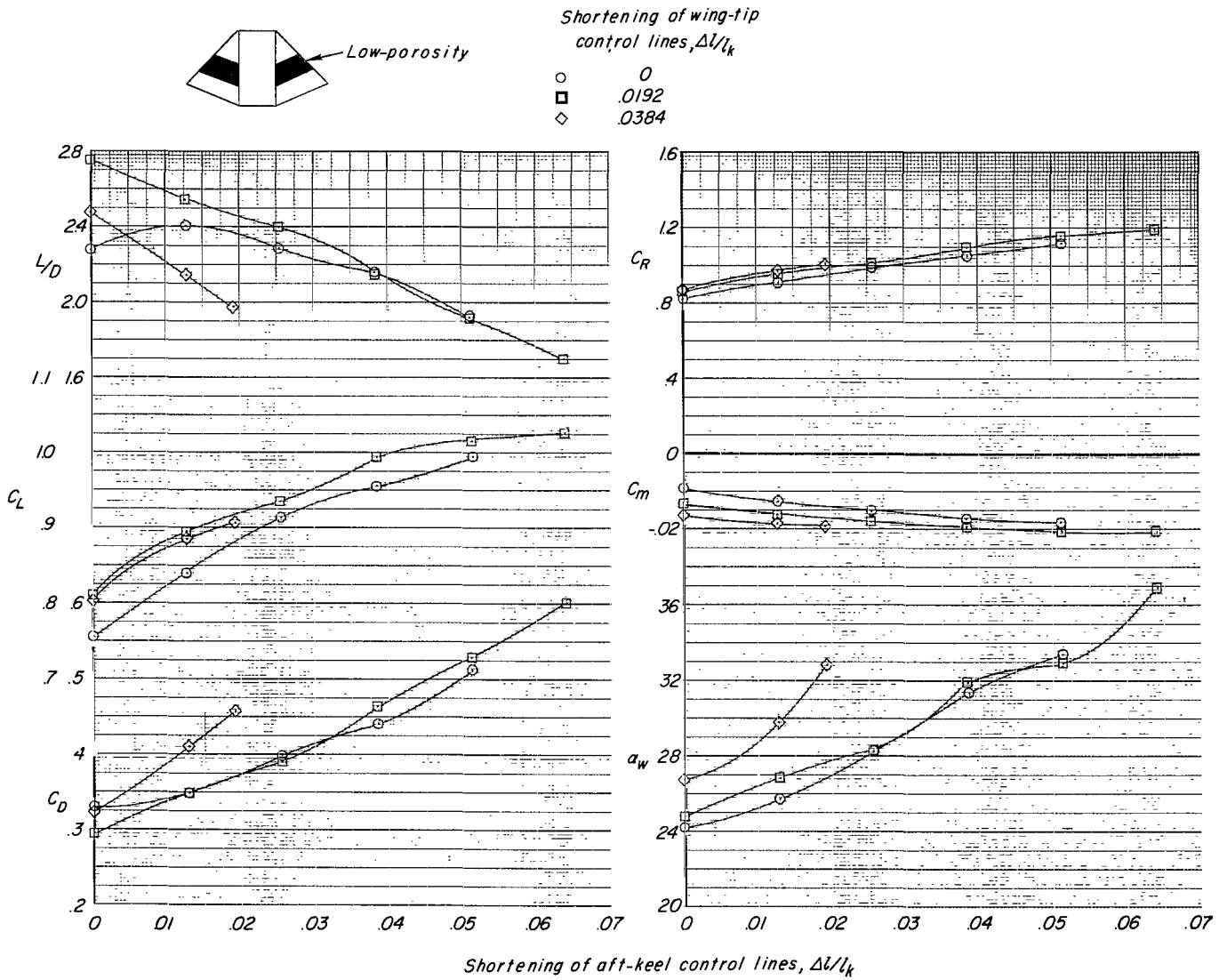

(b) Model B.

Figure 9.- Continued.

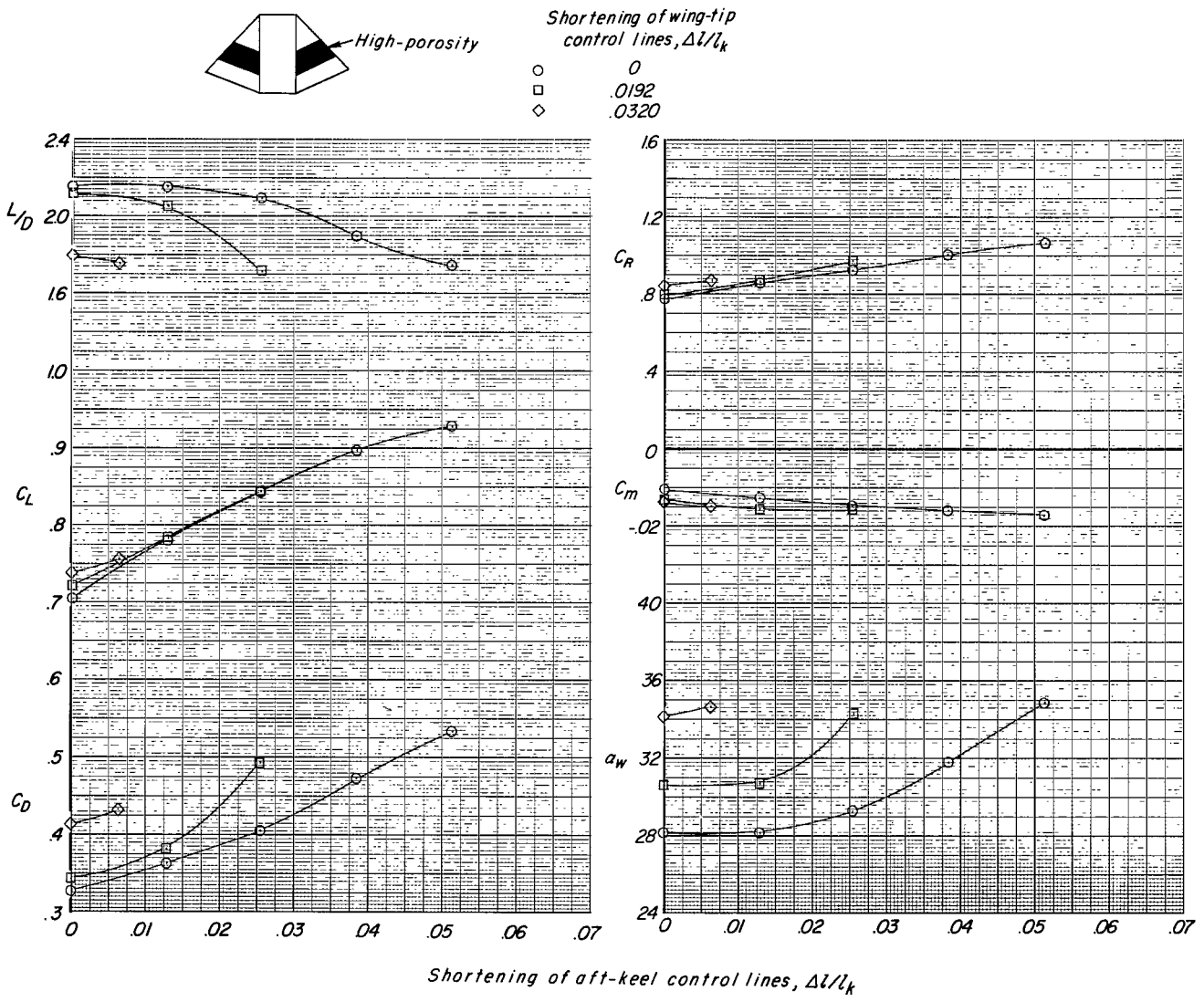

(c) Model C.

Figure 9.- Continued.

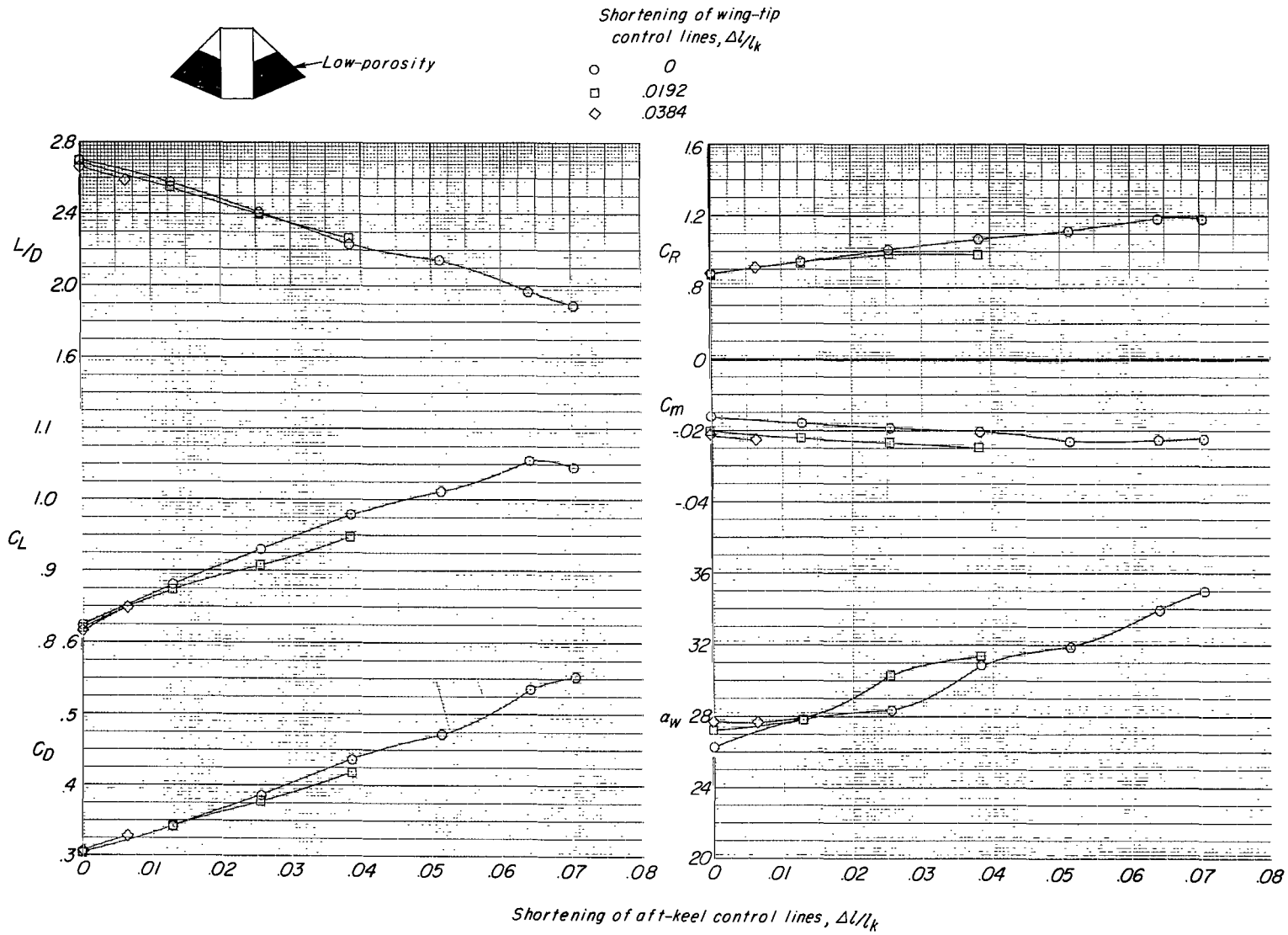

(d) Model D.

Figure 9.- Continued.

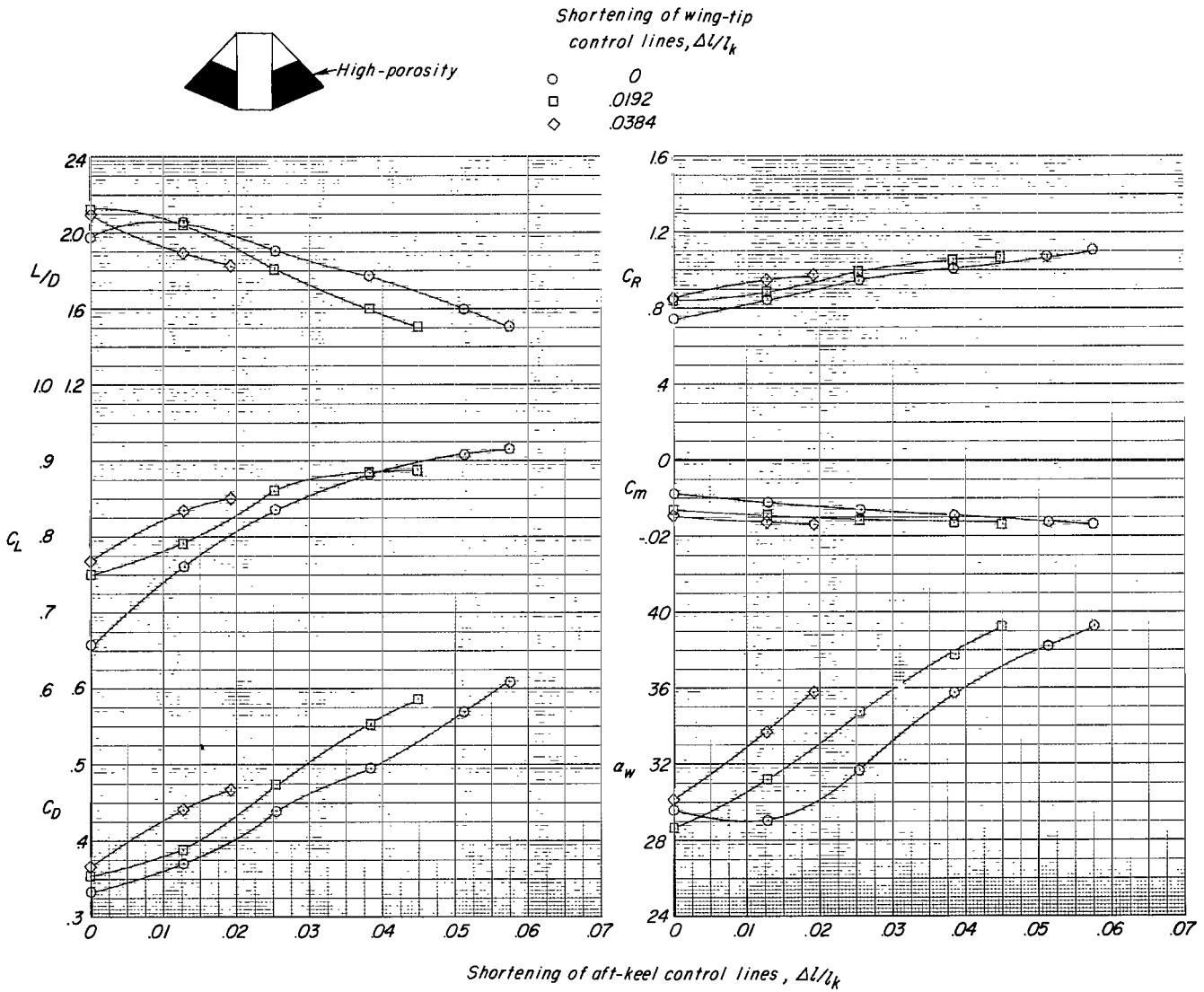

(e) Model E.

Figure 9.- Concluded.

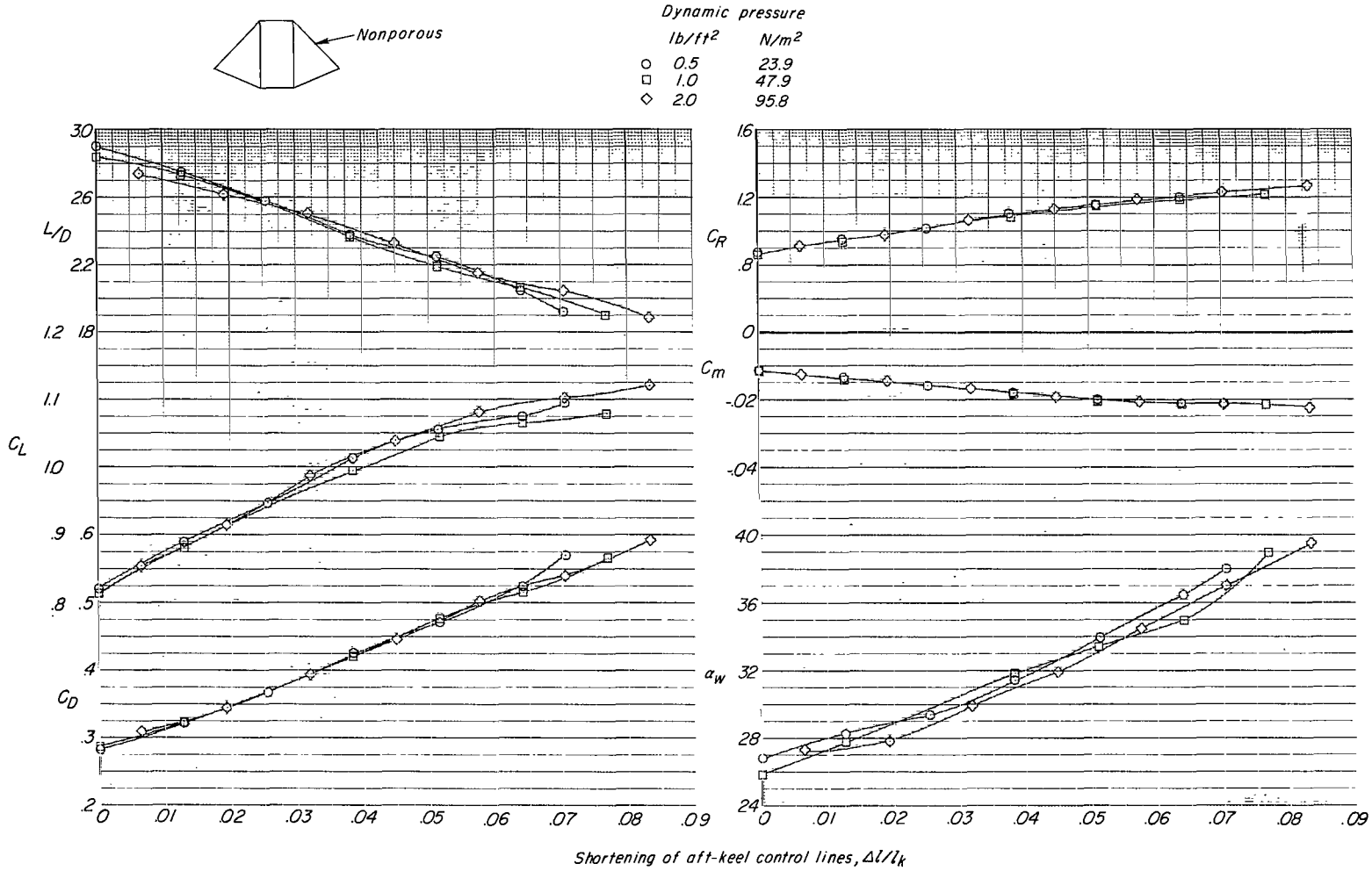

(a) Model A.

Figure 10.- Effects of an increase in dynamic pressure on longitudinal aerodynamic characteristics of a twin-keel all-flexible parawing with various amounts and permeabilities of porous material in outer lobes. Shortening of wing-tip control lines, $\Delta l/l_k = 0$.

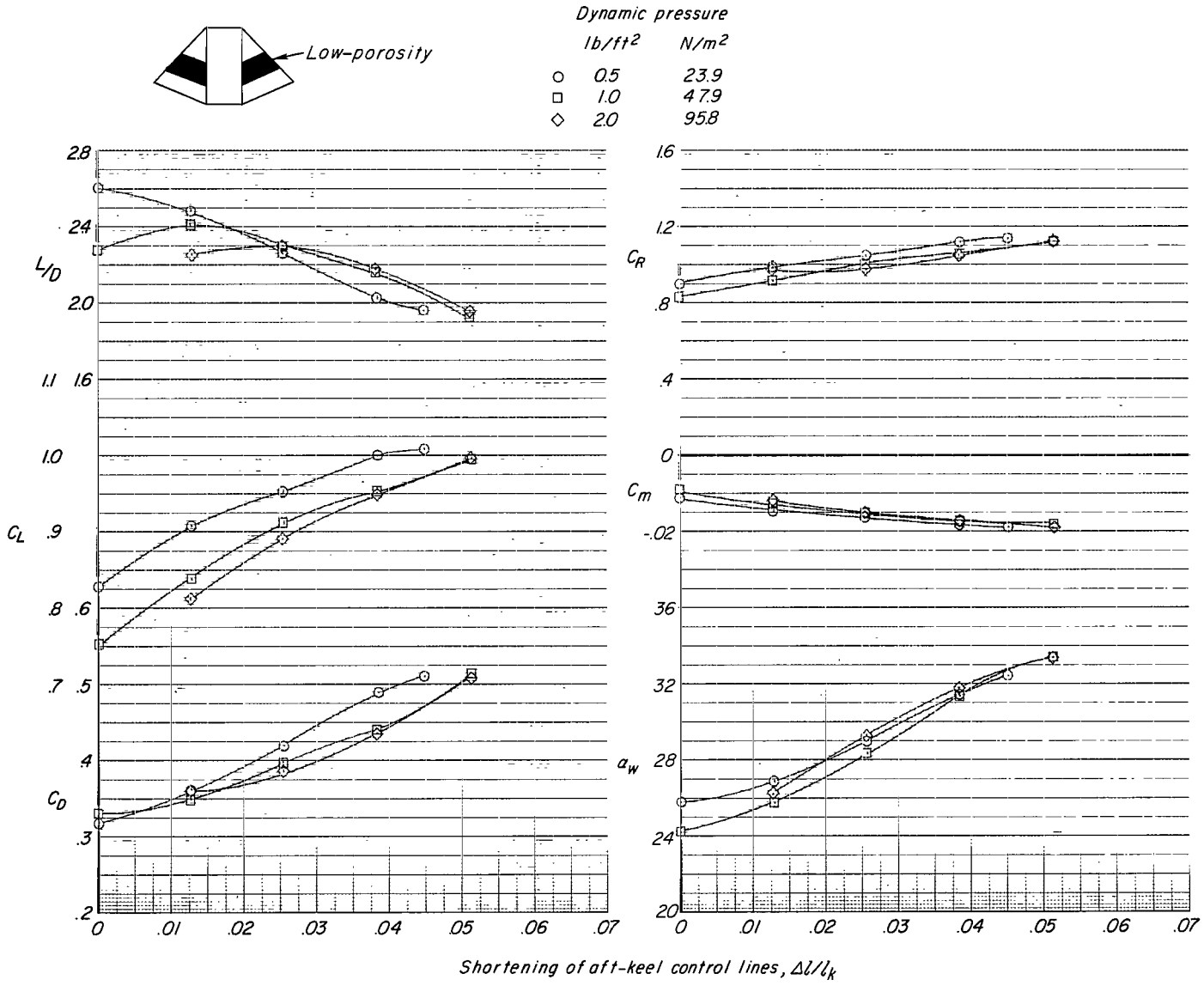

(b) Model B.

Figure 10.- Continued.

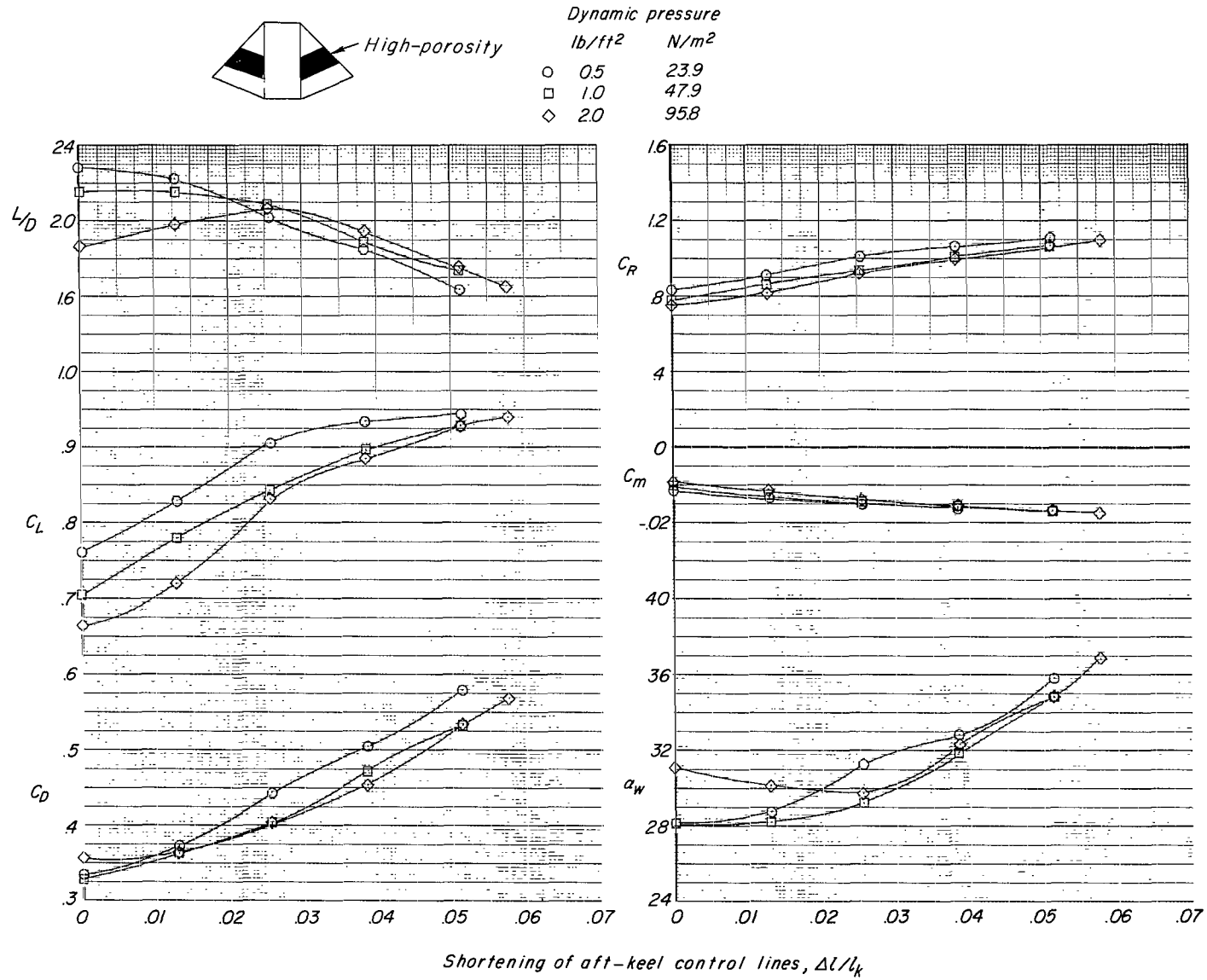

(c) Model C.

Figure 10.- Continued.

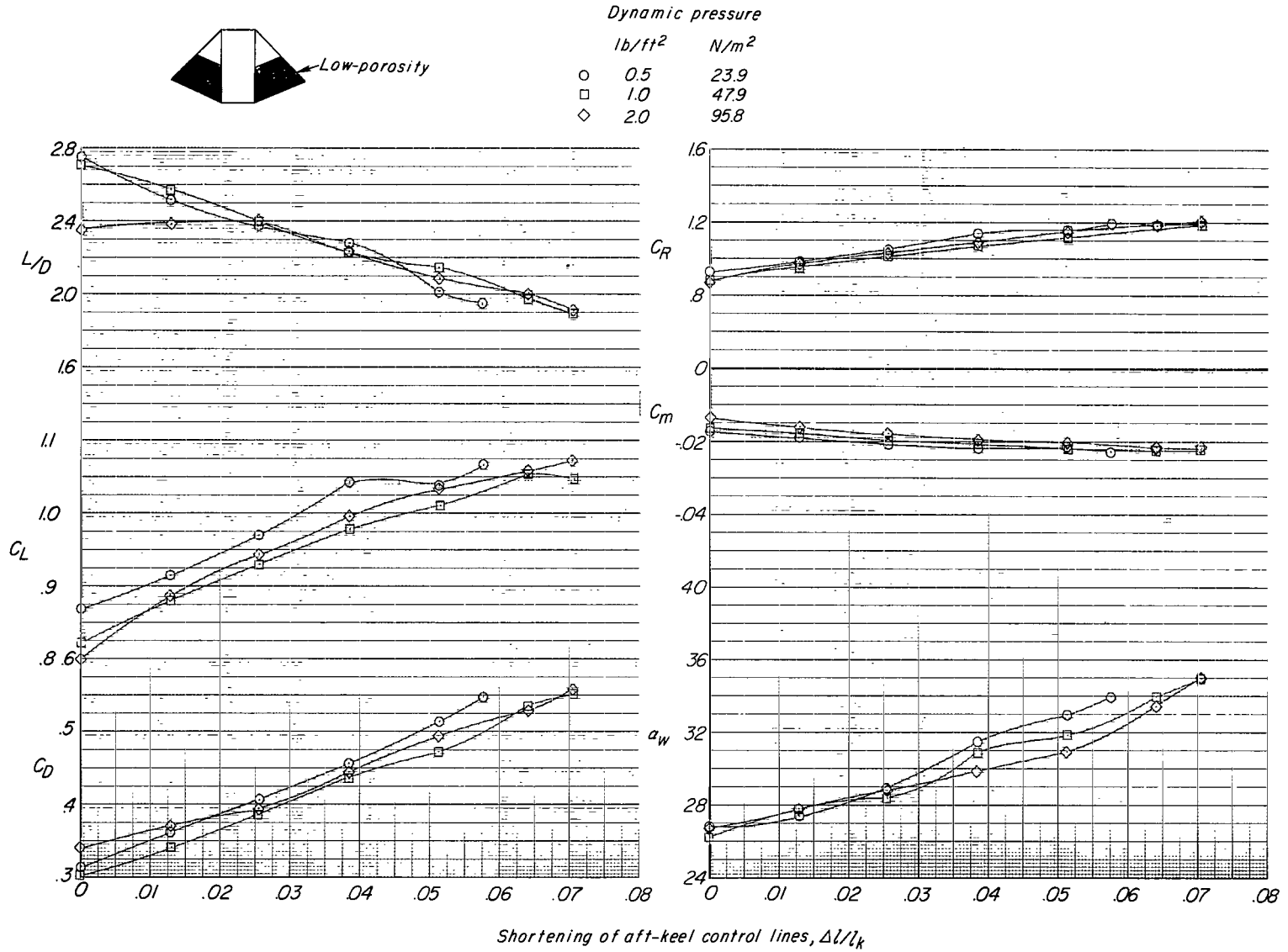

(d) Model D.

Figure 10.- Continued.

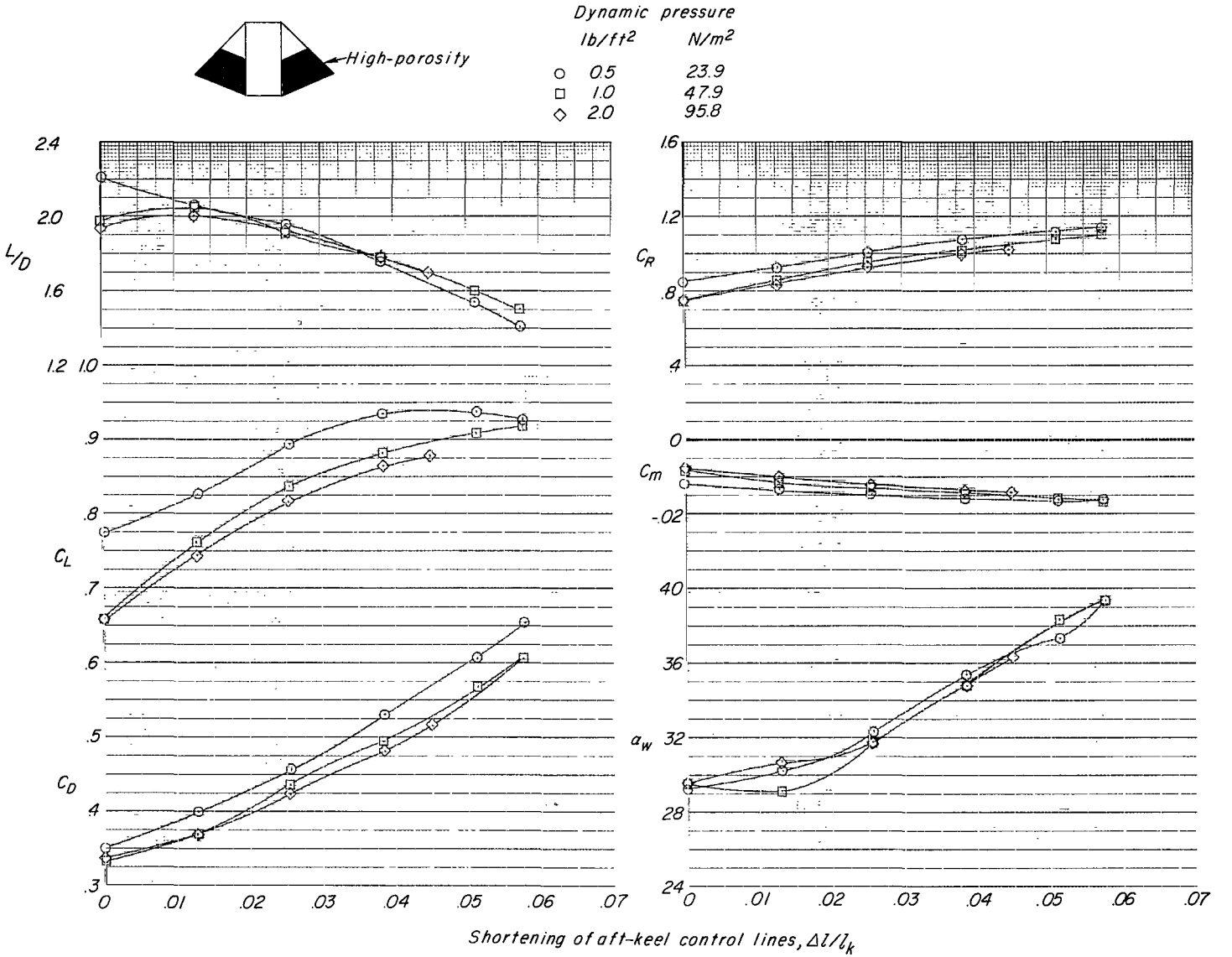

(e) Model E.

Figure 10.- Concluded.

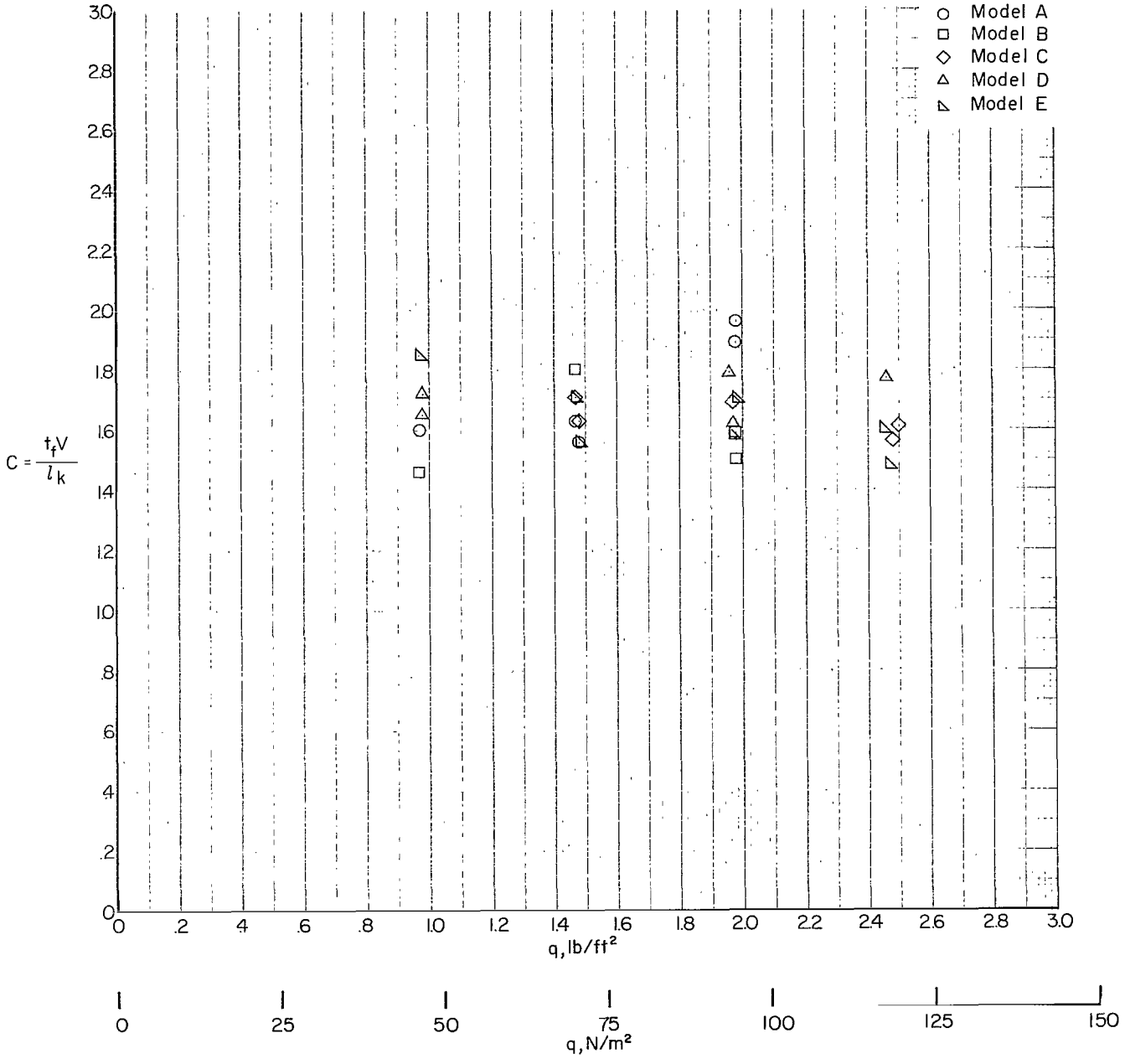

Figure 11.- The variation of the fill-time constant with dynamic pressure.

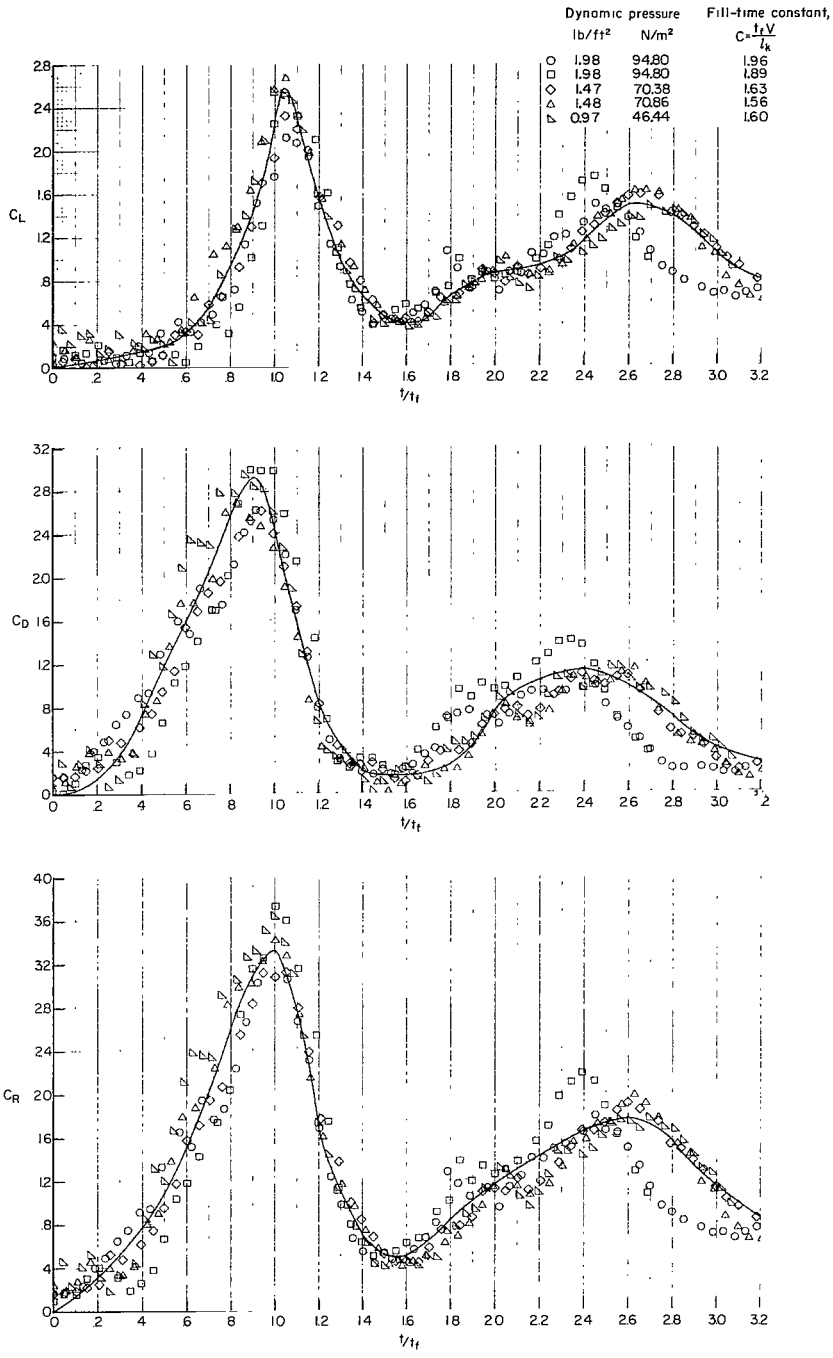

(a) Model A.

Figure 12.- Time histories of lift, drag, and resultant-force coefficient of a twin-keel all-flexible parawing with various amounts and permeabilities of porous materials in the outer lobes.

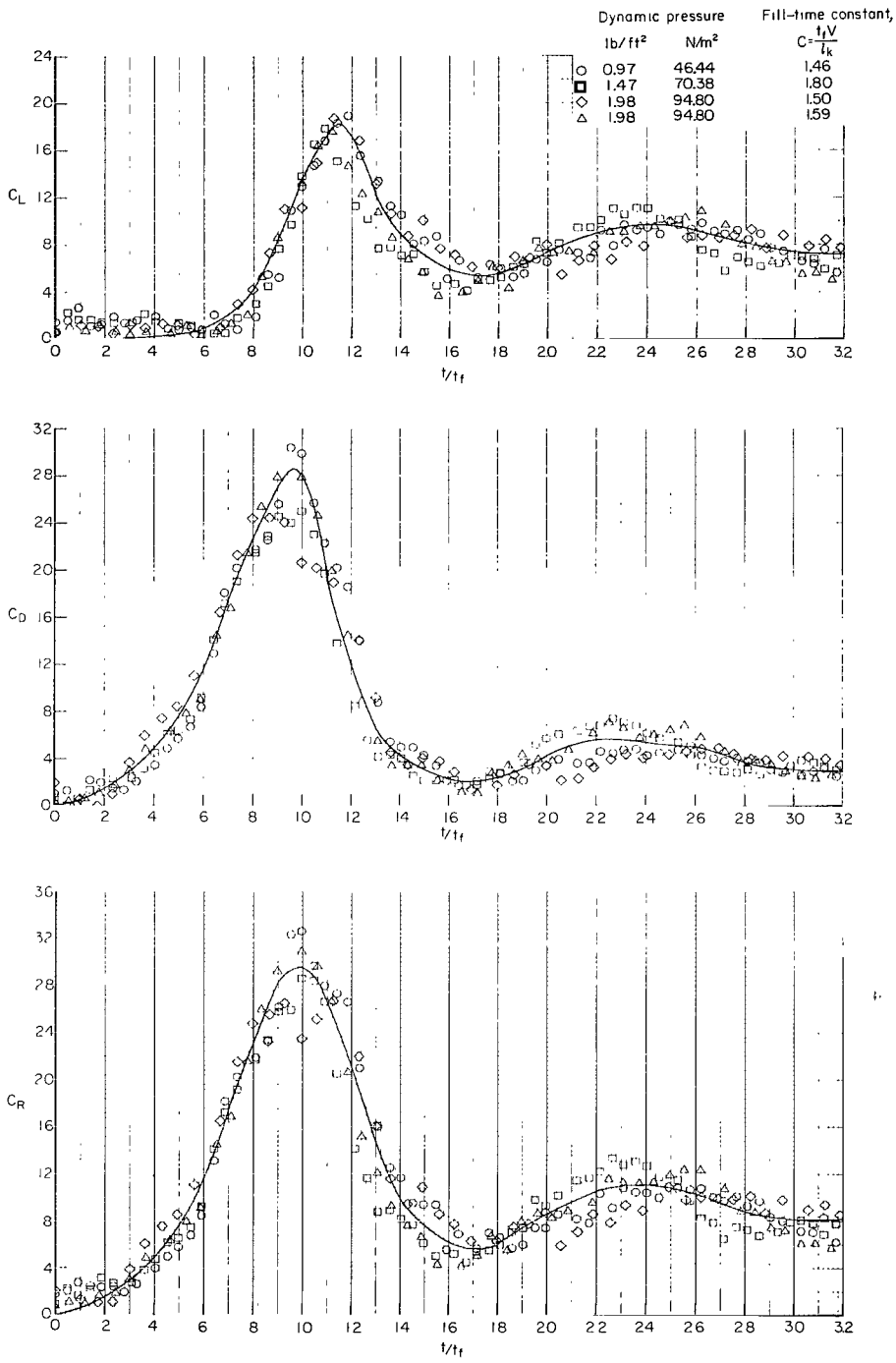

(b) Model B.

Figure 12.- Continued.

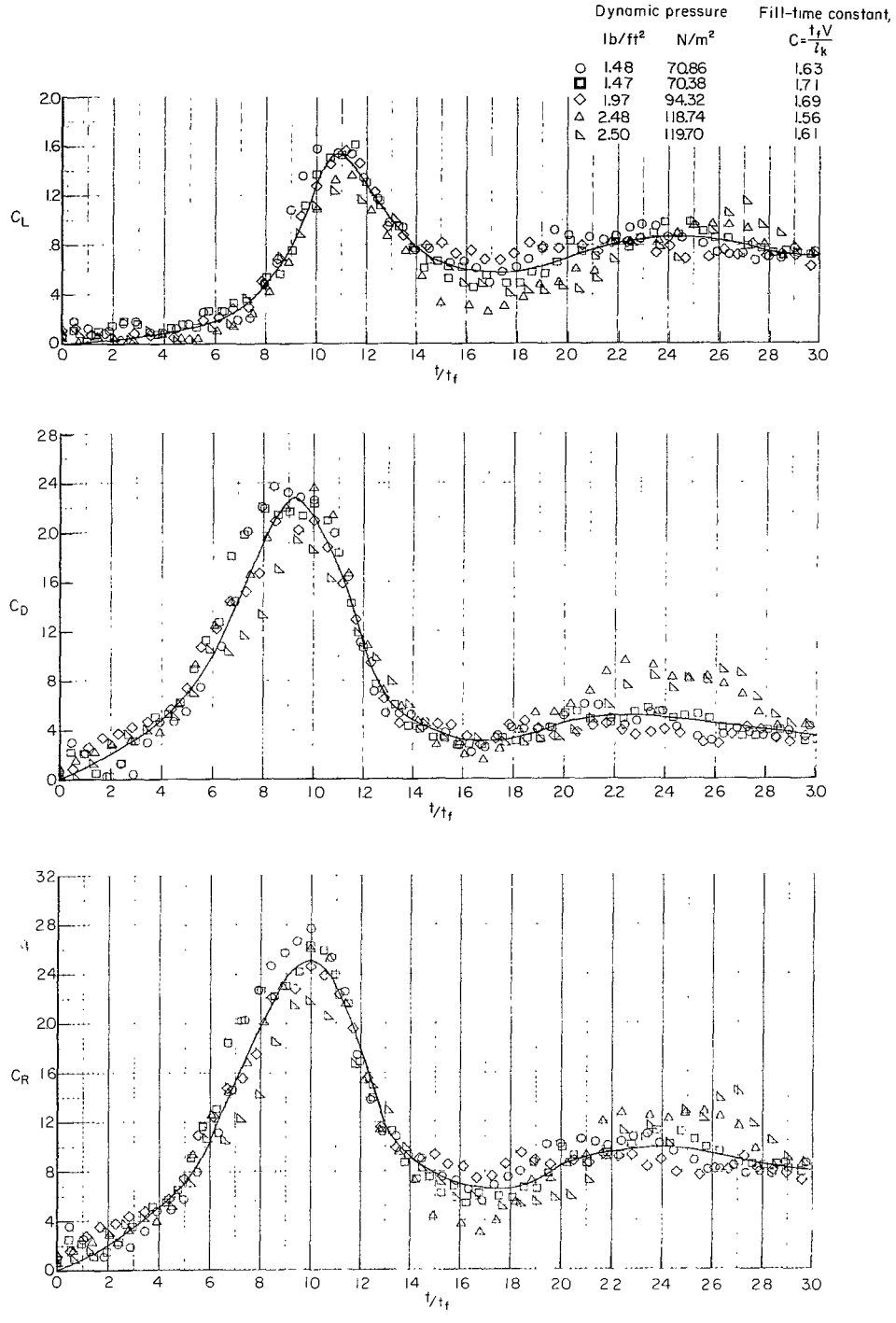

(c) Model C.

Figure 12.- Continued.

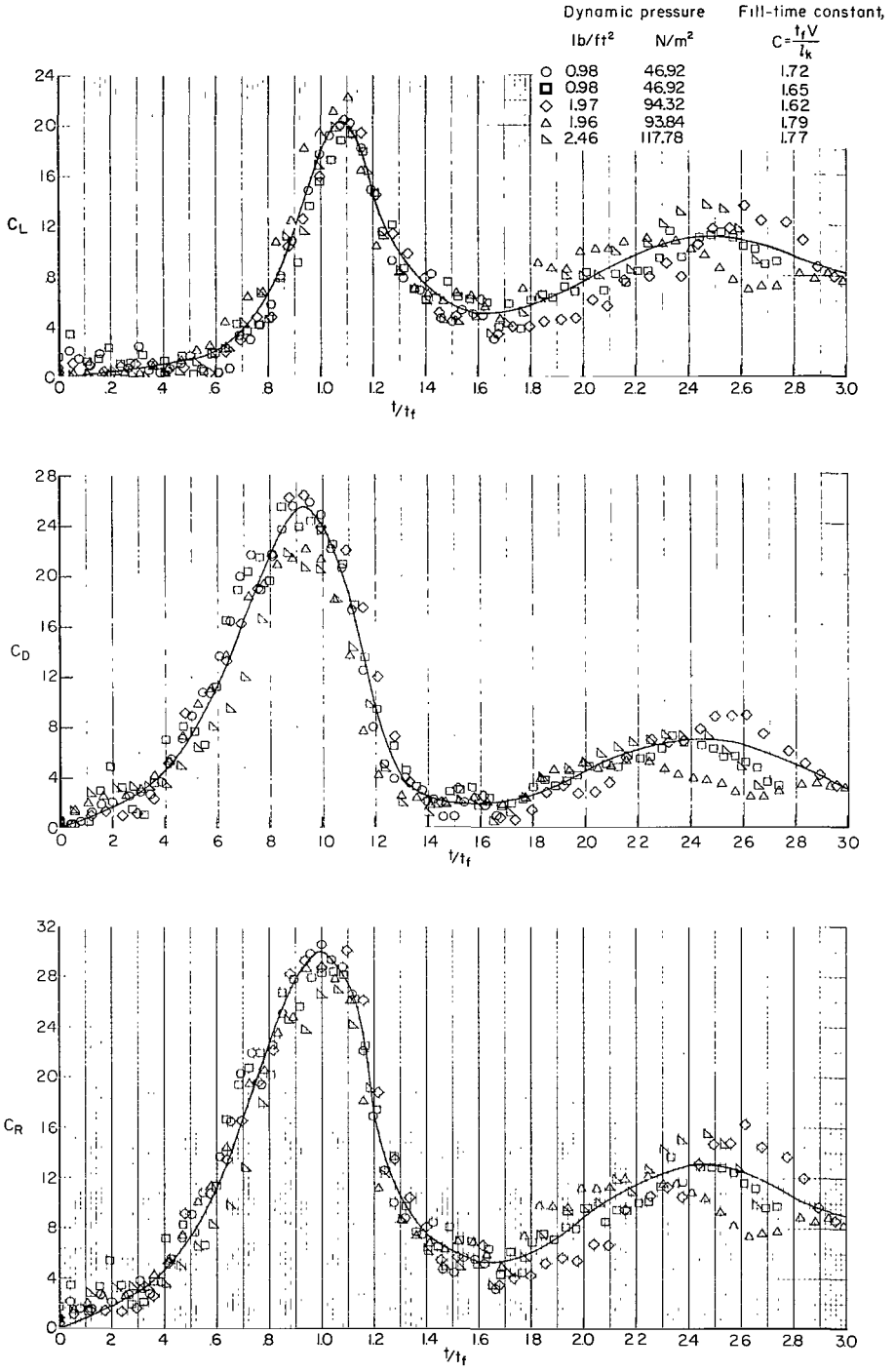

(d) Model D.

Figure 12.- Continued.

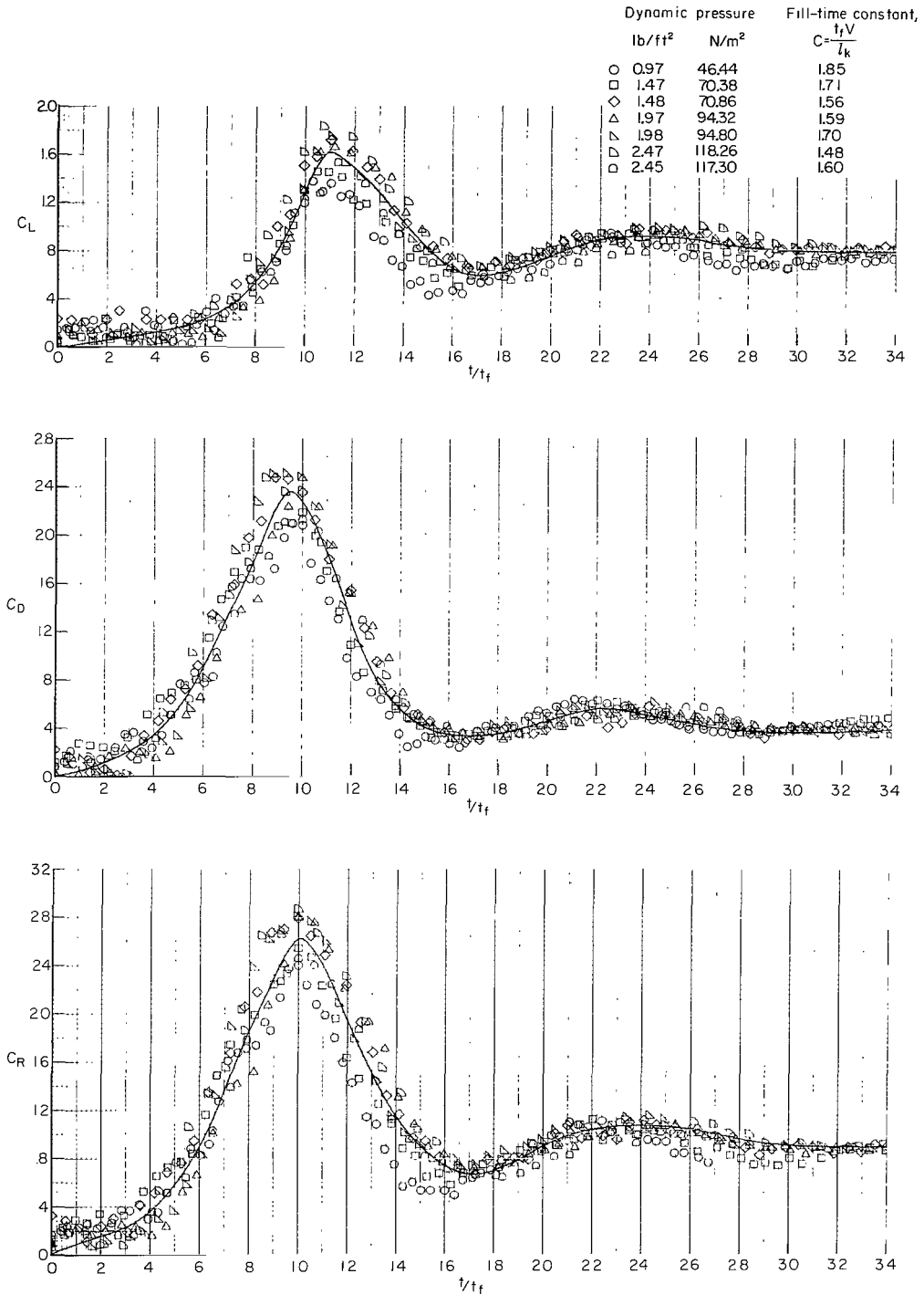

(e) Model E.

Figure 12.- Concluded.

NASA-Langley, 1970 —— 1 L-6961

"The aeronautical and space activities of the United States shall be conducted so as to contribute . . . to the expansion of human knowledge of phenomena in the atmosphere and space. The Administration shall provide for the widest practicable and appropriate dissemination of information concerning its activities and the results thereof."

—NATIONAL AERONAUTICS AND SPACE ACT OF 1958

NASA SCIENTIFIC AND TECHNICAL PUBLICATIONS

TECHNICAL REPORTS: Scientific and technical information considered important, complete, and a lasting contribution to existing knowledge.

TECHNICAL NOTES: Information less broad in scope but nevertheless of importance as a contribution to existing knowledge.

TECHNICAL MEMORANDUMS: Information receiving limited distribution because of preliminary data, security classification, or other reasons.

CONTRACTOR REPORTS: Scientific and technical information generated under a NASA contract or grant and considered an important contribution to existing knowledge.

TECHNICAL TRANSLATIONS: Information published in a foreign language considered to merit NASA distribution in English.

SPECIAL PUBLICATIONS: Information derived from or of value to NASA activities. Publications include conference proceedings, monographs, data compilations, handbooks, sourcebooks, and special bibliographies.

TECHNOLOGY UTILIZATION PUBLICATIONS: Information on technology used by NASA that may be of particular interest in commercial and other non-aerospace applications. Publications include Tech Briefs, Technology Utilization Reports and Notes, and Technology Surveys.

Details on the availability of these publications may be obtained from:

SCIENTIFIC AND TECHNICAL INFORMATION DIVISION

NATIONAL AERONAUTICS AND SPACE ADMINISTRATION

Washington, D.C. 20546